Biochemistry and Biophysics Reports 41 (2025) 101952

Contents lists available at ScienceDirect

Biochemistry and Biophysics Reports

journal homepage: www.elsevier.com/locate/bbrep

Identification and assessment of hub genes and miRNAs coregulatory associated with immune infiltrations and drug interactions in latent tuberculosis based on MicroarrayData analysis, molecular docking, and dynamic simulation

PhongSon Dinh [a,*], ChauMyThanh Tran [a], ThiPhuongHoai Dinh [b], Hai-Anh Ha [a], Aigul Utegenova [c,**], Awais Ali [d,***], Abdulaziz Alamri [e]

[a] College of Medicine and Pharmacy, Duy Tan University, Danang, 550000, Viet Nam
[b] Department of Neurosurgery, Hue University Hospital, Hue University of Medicine and Pharmacy, Hue University, Hue, 530000, Viet Nam
[c] Department of Microbiology and Virology, Astana Medical University, Astana, 010000, Kazakhstan
[d] Department of Biochemistry, Abdul Wali Khan University Mardan, Mardan, 2300, Pakistan
[e] Department of Biochemistry, College of Science, King Saud University, Riyadh, 11451, Saudi Arabia

ARTICLE INFO

Keywords:
Bioinformatics
Biomarkers
Molecular dynamic simulation
MM-GBSA
Latent tuberculosis

ABSTRACT

Tuberculosis (TB) remains a major global health concern, with the transition from latent to active TB still poorly understood. Therefore, enhancing clinical management and prevention strategies for TB is essential. High-throughput sequencing data of genes and miRNAs from individuals at different TB stages were obtained from NCBI. Differential expression analysis was performed using the R package limma, alongside GO and KEGG analyses. The central regulatory network of miRNAs was visualized with Cytoscape, and relevant genes were validated using ROC analysis. The predicted key genes involved in the transition from latent to active TB, including PLEKHG1, CLPB, DOK4, IL1β, and TLR3, are primarily associated with multicellular organism processes, stimulus-response, GPCR ligand binding, and immune functions. Finally, we screened Celastrol and Cefaclor Anhydrous targeting IL1β as potent anti-inflammatory drug to reduce the inflammation due to TB. These findings were further validated with Molecular dynamic simulation MM-GBSA and PCA analysis. Our study advances the understanding of latent tuberculosis and identifies genes and microRNAs as potential biomarkers for diagnosis, monitoring, and treatment, with broader implications for complex disease research.

1. Introduction

Tuberculosis (TB), caused by *Mycobacterium tuberculosis* (*Mtb*) infection, is considered a major cause of infection-related morbidity and mortality worldwide [1]. It is ranked 13th among the leading causes of death and is the 2nd deadliest infectious agent after COVID-19, surpassing even HIV/AIDS [2]. Vietnam is one of the countries suffering from high rates of tuberculosis and is among 30 countries with the highest rates of multi-drug-resistant tuberculosis. In 2021, there were more than 172,000 TB cases and 10,400 deaths attributed to tuberculosis [2].

Tuberculosis can exist in two clinical stages: latent tuberculosis (latent TB or LTB) and active tuberculosis (active TB or ATB) [3]. Approximately a quarter of the global population is considered to have LTB infection, but current diagnostic tests lack of ability to determine whether these individuals will remain LTB carriers for life or are at risk of progressing to ATB. Approximately 5–10 % LTB individuals will develop ATB within the first five years of infection if no treatment is received [4]. The risks of LTB becoming ATB depends on several factors, including the status of the immune system [5–7]. In fact, early LTB treatment is beneficial for both individuals and community. Identifying the immune responses associated with LTB is critical to understand ?

* Corresponding author.
** Corresponding author.
*** Corresponding author.
E-mail addresses: dinhphongson@dtu.edu.vn (P. Dinh), trancmythanh@dtu.edu.vn (C. Tran), phuonghoai1412.md@gmail.com (T. Dinh), hahaianh@dtu.edu.vn (H.-A. Ha), Utegenova.aigul.amu@gmail.com (A. Utegenova), Awaisalibio@gmail.com, awaisali@awkum.edu.pk (A. Ali), abalamri@ksu.edu.sa (A. Alamri).

https://doi.org/10.1016/j.bbrep.2025.101952
Received 1 November 2024; Received in revised form 1 February 2025; Accepted 9 February 2025

why most people can contain the disease and stay at the latent stage, while others develop ATB. The transcriptomic data analysis of whole blood in tuberculosis has proven useful in distinguishing ATB cases from other cohorts, such as LTB or uninfected individuals. However, gaining insights into what type of immune responses involved in controlling tuberculosis, particularly LTB, is still a challenge [8]. Some evidences highlighted the mechanistic role of T cells in controlling tuberculosis infection [9]. In particular, T-cell responses specifically to TB have been shown to be vital for body protection in the context of both naturally acquired infection [10] and vaccination [8,11,12]. Among many factors involved in LTB, dendritic cells (DCs) are one of the decisive components of the immune response to *Mtb* [13]. Nonetheless, current knowledge about the roles of variouscomponents of human DCs in shaping specific T-cell responses during latent stage is still limited [14]. In comparing the differentiation of DCs among ATB, LTB and healthy donors, researchers found that the differentiation of DCs in LTB patients was significantly higher than that in ATB patients, suggesting that DCs differentiation is impaired in ATB patients. In addition, a selective activation of circulating DCs was also observed in LTB patients. By investigating the molecular basis of changes in differentiation program, the authors reported a set of down-regulated genes related to the IFN-α/β signaling, DCs maturation and the antigen presentation, as well as the upregulation of *Mtb*-exposed DC. This emphasises the association between the altered developmental profile of DCs in ATB patients and the remarkable alterations in the IFN-α-related molecular signals that mediate antigen presentation and the generation of an antigen-specific T-cell response. These data thus highlight the indispensable role of IFN-α in determining the induction of *Mtb*-specific immunity, which is essential for cotrolling *Mtb* infection [14]. On the other hand, *Mtb* has also developed specialized mechanisms to parasitize macrophage cells. These mechanisms include the production of various antioxidants regulated by the transcription factor SigH [15], the interference to phago-lysosomal fusion and acidification [16,17] and the production of IFN-gamma (IFN-γ) [18]. These mechanisms allow *Mtb* to overcome the rapid generation of reactive oxygen species (ROS). known as oxidative burst, and survive after the host's inflammatory responses. When *Mtb* infection in most exposed individuals is controlled, it persists in an asymptomatic form known as LTB [19]. Some evidence highlights the mechanistic role of T-cells in controlling tuberculosis infection [9]. In particular, TB-specific T-cell responses have been shown to be vital for the body protection in the context of naturally acquired infection [10] and vaccination [8,11,12].

To the best of our knowledge, there is still no "gold standard" test for latent TB diagnosis. The two traditional tests recommended by the WHO for latent TB infection are the Mantoux Tuberculin Skin Test (TST or Mantoux test) and Interferon Gamma Release Assays (IGRAs) [20,21]. However, both TST and IGRAs, are limited in predicting the likelihood of LTB individuals becoming ATB. In addition, the TST false positive may occur due to cross-activity with non-tuberculous mycobacteria or Bacille Calmette-Guerin (BCG) vaccination, unless the individual was vaccinated with BCG more than 10 years ago [22]. Although the IGRA has higher specificity, and less crossed-activity, its application in low- and mid-income countries is not recommended due to its high cost [23]. Recently, Xpert MTB/RIF and Xpert Ultra have been included in WHO guidelines as initial tests for TB diagnosis [24]. These tests enable clinicians to quickly diagnose the presence of *Mtb* in patient sputum using realtime PCR, and also to detect the presence of rifampicin-resistant *Mtb* with a relatively low cost. However, their sensitivity is suboptimal, and these tests were not designed to predict the risk of progression from LTB to ATB [25]. Hence, characterizing the molecular components of the immune response that protecthuman against tuberculosis may help to develop better diagnostic measures and more effective therapeutic interventions. In this study, the GSE datasets collected from NCBI were analyzed in order to characterize the expression of genes and miRNAs involved in immune response of healthy control (HC), LTB, and ATB. This study was expected to provide a deeper understanding of the mechanism by which the human body responds to these infectious agents at the molecular level, which cannot be fully achieved using-traditional whole-blood methods.

2. Materials and methods

2.1. Bioinformatics analysis of miRNA and mRNA expression changes

R software version 4.1.1 (R Foundation for Statistical Computing, Vienna, Austria) was used to performed data analysis (http://www.R-project.org), Perl software (https://www.perl.org/), and custom analysis code, with a LogFC cut-off >0.5 and p-value <0.05 for miRNA differential expression via the *limma* package [26]. Bioinformatics analysis data was sourced from the Biotechnology Information Center of the US National Institutes of Health's Library of Medicine (https://www.ncbi.nlm.nih.gov/). The search used "Latent tuberculosis" as the keyword to identify high-throughput sequencing datasets. Criteria included detection of miRNAs and mRNAs in immune cells such as dendritic cells (DC), monocytes (Mono), and peripheral blood mononuclear cells (PBMC). Selected GSE datasets required data from more than 3 blood samples from healthy, latent TB, and active TB groups. The selection criteria for CD4, CD8 T cells, DCs and PBMCs from control and patients groups adhered to the diagnostic criteria outlined in each GSE data series (Fig. 1).

2.2. Prediction of miRNA/mRNA networks

Cytoscape software version 3.10.0 (http://cytoscape.org/) [27] was employed to predict the 3′UTR region of mRNA targets of selected miRNA via cyTargetLinker (https://cytargetlinker.github.io/) [28]. R coding was performed to detected mRNA dysregulation using GSE databases (https://www.ncbi.nlm.nih.gov/geo/) [29], which is crucial for our research given the potential miRNA-induced mRNA reduction. The Venny tool was used to identify mRNA intersection points from the datasets (https://bioinfogp.cnb.csic.es/tools/venny/) [30], and Cytoscape software was applied to construct the miRNA/mRNA interaction network.

2.3. Gene ontology (GO) and Kyoto encyclopedia of genes and genomes (KEGG)

GO gene function annotation is useful in analyzing the functional significance of differentially expressed genes. KEGG signaling pathways show notable enrichment in differentially expressed genes compared to the genomic background, highlighting potential active pathways in TB progression. Utilizing the "clusterProfiler" package in R software (Version 4.1.1) enables efficient KEGG enrichment analysis to identify these key pathways (https://bioconductor.org/packages). was used to analyze GO and KEGG [31]. This study utilized R and Perl software to convert TB-relevant gene IDs to entrez IDs for GO and KEGG analysis, predicting biological processes, cellular components, molecular functions, and signaling pathways. The aim was to elucidate the primary roles of these genes in the development of latent tuberculosis.

2.4. Analysis of the ROC curve and estimate the area under the ROC curve

In the study, R software, Perl tools, Venny tools, and analysis code were used to validate the diagnostic potential of miRNAs and mRNAs related to latent tuberculosis from the GSE dataset assessing their sensitivity and specificity based on molecular expression.

2.5. Target drugs and molecular docking

The Drug Gene Interaction Database (DGIdb, https://dgidb.org/) version 5.0, as detailed in the latest publication (Nucleic Acids Research,

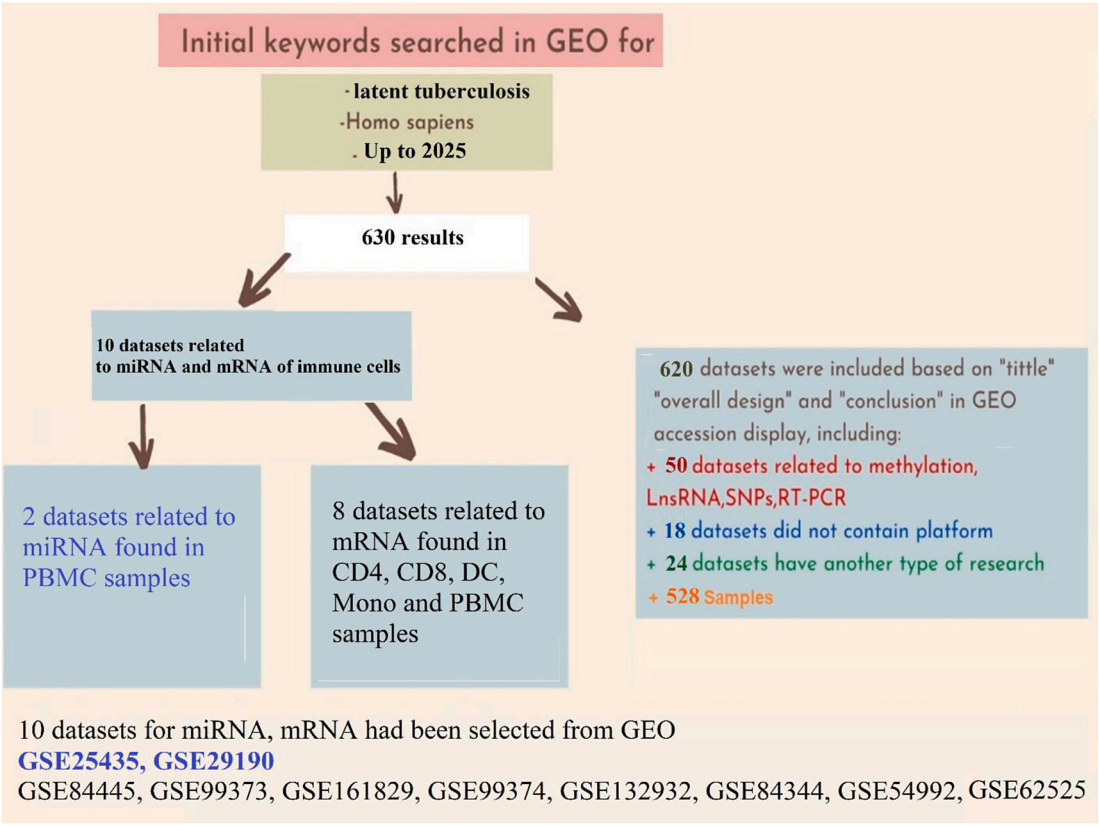

Fig. 1. Research methodology diagram.

2024), was utilized to identify potential drugs targeting cuproptosis-related genes in latent tuberculosis. DGIdb integrates a wide range of sources, including ChemIDplus, HemOnc, NCIt, Drugs@FDA, HGNC, and RxNorm, providing a robust resource for precision medicine and drug discovery. The addition of a GraphQL API and modular data normalization ensures enhanced data accessibility, usability, and reproducibility, making it a reliable tool for identifying drug–gene interactions [32]. Molecular modeling and molecular docking were conducted to investigate the binding affinities and interaction patterns of potential inhibitors against the target protein. The initial step involved the conversion of Simplified Molecular Input Line Entry System (SMILES) codes for the compounds of interest into three-dimensional (3D) structures. This conversion was facilitated using Open Babel, an open-source tool for chemical data manipulation, which also performed energy minimization on the generated 3D structures to prepare them for subsequent docking simulations.

AutoDock Vina [33] a widely recognized software for molecular docking, was employed to perform the docking simulations. The protein model used for docking was obtained from the RCSB Protein Data Bank (PDB) with the PDB code 9ILB, which represents the target protein structure. AutoDock Vina was configured to search for optimal docking poses within a defined grid box centered at coordinates (−14.62, 13.26, −1.35), which was chosen to encompass the active site of the protein. The grid box dimensions were set to 50.00 Å x 40.82 Å x 50.00 Å in the x, y, and z axes, respectively, ensuring sufficient coverage of the protein's conformational space and binding site. The docking simulations were set to explore a maximum of 9 binding modes per ligand, with an energy range of 3 kcal/mol and an exhaustiveness level of 8 to ensure a comprehensive search of the conformational space.

2.6. Molecular dynamic simulation

Molecular dynamics simulations using Schrödinger LLC's Desmond software [34] were conducted for 150 ns (ns) to assess ligand-receptor interactions. These simulations, integral to receptor-ligand docking [35], enabled rigorous analysis of the compounds' binding against the target protein. By employing Newton's classical equation of motion [36], the MD simulations provided insights into ligand binding under physiological conditions.

The selected proteins and ligands underwent optimization and minimization using Maestro's Protein Preparation Wizard, removing steric clashes, bad contacts, and distorted geometries. Systems were built with the System Builder tool using TIP3P solvent model in an orthorhombic box with OPLS_2005 force field [37]. Counter ions were added for neutralization, and 0.15 M sodium chloride was included to mimic physiological conditions at 300K temperature and 1 atm pressure. Trajectories were stored every 100 ps (ps), and protein-ligand stability was assessed through Root Mean Square Deviation (RMSD) analysis and Root mean square fluctuation (RMSF).

2.7. Molecular mechanics and generalized born surface area (MM-GBSA) calculations

MM-GBSA analysis, conducted using the prime module of Schrödinger, evaluated binding free energy (ΔG_{bind}) for ROCK2 complexed with A1 and [38]. Counter ions were removed, employing the VSGB solvent model with OPLS 2005 force field and rotamer search techniques to calculate ΔG_{bind}. Calculations utilized MD trajectory frames at 10ns intervals post-MD run. The total binding free energy (ΔG_{bind}) was determined as the difference between the energy of the protein-ligand complex ($G_{complex}$) and the free energies of the individual protein ($G_{protein}$) and inhibitor (G_{ligand}), as described in Eqs (1) and (2) [39].

$$\Delta G_{bind} = G_{complex} - (G_{protein} - G_{ligand}) \quad (1)$$

$$\Delta G_{bind} = \Delta E_{gass} + \Delta Gs_{ol} - T\Delta S \text{----------} \quad (2)$$

$$\Delta E_{gas} = \Delta E_{int} + \Delta E_{ELE} + \Delta E_{VDW} \text{----------} \quad (3)$$

$$\Delta Gs_{ol} = \Delta G_{polar} + \Delta G_{nonp} = (\Delta G_{GB} - \Delta G_{s}) \text{----------} \quad (1)$$

$$T\Delta S = T(\Delta S_{trans} + \Delta S_{rot} + \Delta S_{vib}) \text{----------} \quad (5)$$

The gas phase interaction energy (ΔE_{gas}) is calculated as the sum of van der Waals and electrostatic energy terms, where internal energy is omitted (Eq (3)). Solvation free energy (ΔG_{sol}) is determined by adding polar (generalized born) and nonpolar energy (solvent accessible surface area) contributions (Eq (4)) [36]. The term TΔS represents conformational entropy, incorporating translational, rotational, and vibrational entropy changes upon binding (Eq (5)) [36].

2.8. Principal component analysis (PCA)

Principal component analysis (PCA) and dynamic cross-correlation matrix (DCCM) of each complex from MD simulation trajectories was conducted using the bio3d package utilizing the R-Project [40] and ProDy software [41]. This statistical method analyzes significant fluctuations in protein residues by examining the covariance matrix of alpha-carbon (Cα) atoms. The eigenvectors with the highest eigenvalues are deemed principal components, with three major components considered for this study. PCA provides insight into protein dynamics by calculating these principal components.

2.9. Ethics statement

The scientists contributing to this database have received ethical approval according to the declaration of Helsinki.

3. Results

3.1. Screening and selecting datasets for analysis

A comprehensive search of the NCBI website revealed that as of 2025, 630 datasets related to tuberculosis (TB) were available. For next step, we identified datasets related to circulating miRNA and mRNA in immune cells isolated from non-invasive biopsy samples, including $CD4^+$ T cells (CD4), $CD8^+$ T cells (CD8), dendritic cells (DC), monocytes (Mono) and peripheral blood mononuclear cells (PBMCs). These cells are key components of the immune responses against bacterial invasion [42]. Datasets involving LncRNA, circRNA, SNPs, cultured cells and single sample analyses were excluded. As a result, among 622 datasets, 8 data sets containing high-throughput mRNA sequencing data analysis of CD4, CD8, DC, Mono and PBMC samples were selected, including: GSE84445, GSE99373, GSE161829, GSE99374, GSE132932, GSE84344, GSE54992 and GSE62525. In addition, 2 other datasets, GSE25435 and GSE29190, related to miRNAs in PBMC samples were also selected. Those 10 datasets provide a comprehensive view of TB-related miRNA and mRNA expression profiles as reported in the Gene Expression Omnibus (GEO) database (Table 1).

3.2. Prediction of potential molecular markers in the progression of latent tuberculosis

Fig. 2 illustrates the differentially expressed genes, both upregulated and downregulated, across the three study groups. These results were analyzed from the datasets listed in Table 2. Our data analysis of high-throughput sequencing results revealed differential expression of miRNAs and mRNAs in TB patients (Table 3 and Fig. 2). Through bioinformatics analysis, we classify the results obtained from each dataset to identify potential molecular markers that may play a critical role in the progression of LTB.

Table 1
Information of used GSE datasets with their subject and platform.

GEO accession number		Subjects			Platform
		HC	LTB	ATB	
mRNA	GSE84445	20	20	0	GPL16791 Illumina HiSeq 2500 (*Homo sapiens*)
	GSE99373	19	20	0	GPL16791 Illumina HiSeq 2500 (*Homo sapiens*)
	GSE161829	20	40	46	GPL24676 Illumina NovaSeq 6000 (*Homo sapiens*)
	GSE99374	20	20	0	GPL16791 Illumina HiSeq 2500 (*Homo sapiens*)
	GSE132932	7	10	0	GPL16791 Illumina HiSeq 2500 (*Homo sapiens*)
	GSE84344	5	5	5	GPL15718 LaRiM Operon Human V3.0 printed oligonucleotide 36K array
	GSE54992	6	6	27	GPL570 [HG-U133_Plus_2] Affymetrix Human Genome U133 Plus 2.0 Array
	GSE62525	14	14	14	GPL16951 Phalanx Human OneArray Ver. 6 Release 1
miRNA	GSE25435	3	3	3	GPL10850 Agilent-021827 Human miRNA Microarray (V3) (miRBase release 12.0 miRNA ID version)
	GSE29190	3	6	6	GPL10850 Agilent-021827 Human miRNA Microarray (V3) (miRBase release 12.0 miRNA ID version)
Total		**117**	**144**	**101**	

Using the online tool Venny 2.1, we search for molecular markers that consistently appeared across multiple datasets, thereby enhancing the reliability of the results in each stage of disease progression (Figs. 3 and 4).

Intersecting the datasets aims to identify potential genes. The simultaneous appearance of a gene across multiple datasets from many different studies enhances the reliability of the gene. Therefore, it may be a molecular marker warranting further consideration.

We could only find two sets of GSE data related to differential expression of miRNAs at different stages of tuberculosis in PBMCs, including GSE25435 (3 HC samples, 3 LTB samples, and 3 ATB samples) and GSE29190 (6 HC samples, 6 LTB samples, and 6 ATB samples), which met the initial screening criteria. The *limma* package was used to analyze miRNA expression differences. To enhance accuracy, we cross 2 sets of data together. The fact that a miRNA appears simultaneously in 2 datasets of different studies indicates a greater reliability, making that miRNA a promising candidate. We use this theoretical basis for selecting potential markers. We analyzed the differential expression of miRNAs in different stages of TB, including HC, LTB, and ATB from 2 GSE datasets related to PBMC. Based on the overlap between these datasets, we predicted potential miRNAs and constructed a miRNA/gene interaction network (Fig. 5). The miRNAs selected for further studyare described in Table 4.

3.3. GO và KEGG analysis

To better understand the functions and interrelationships of these genes, we employed GO enrichment and KEGG pathway analysis as our principal tools. The results of GO analysis included 323 functional terms related to biological process (BP), cellular component (CC), and molecular function (MP) (Fig. 6A). For GO-BP enrichment analysis, the results showed 299 GO terms. Among them, the Top 10 GO terms are GO_1903131 - mononuclear cell differentiation, GO_0031349 - positive regulation of defense response, GO_0050729 - positive regulation of inflammatory response, GO_0030098 - lymphocyte differentiation, GO_0050867 - positive regulation of cell activation, GO_0002253 - activation of immune response, GO_0050727 - regulation of

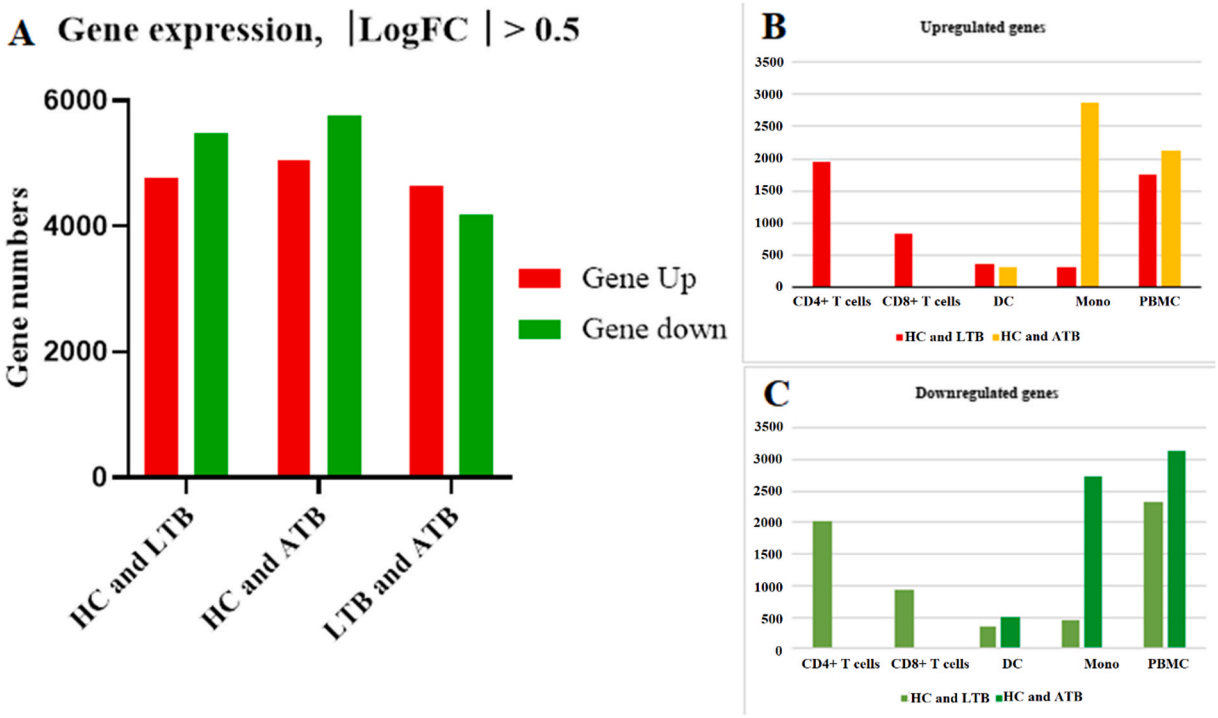

Fig. 2. Comparison of total up- and down-regulated genes across HC, LTB and ATB stages; (A) Total differential gene expressions; (B) Up-regulated genes in five immune cell types comparing HC and LTB stages vs HC and ATB stages; (C) Down-regulated genes in five immune cell types comparing HC and LTB stages vs HC and ATB stages. |logFC|>0.5.

Table 2
Summary of data set statistics comparing CD4 samples between HC and LTB groups.

Compare stage	Type sample	GSE ID	Groups	
			HC	LTB
HC and LTB	CD4	GSE84445	10	10
		GSE99373	19	20
		GSE161829	20	40
	CD8	GSE84445	10	10
		GSE99374	20	20
		GSE132932	7	10
	DC	GSE84344	5	5
	Mono	GSE54992	6	6
	PBMC	GSE62525	14	14
HC and ATB	DC	GSE84344	5	5
	Mono	GSE54992	6	9
	PBMC	GSE62525	14	14

Table 3
Differential gene expression analysis between HC and LTB groups in CD4 samples.

Information			Gene expression, |LogFC| > 0.5	
			Upregulated	Downregulated
HC and LTB	CD4	GSE84445	1370	103
		GSE99373	282	1474
		GSE161829	309	448
	CD8	GSE84445	172	579
		GSE99374	543	165
		GSE132932	132	191
	DC	GSE84344	367	359
	Mono	GSE54992	310	454
	PBMC	GSE62525	1760	2337
HC and ATB	DC	GSE84344	330	512
	Mono	GSE54992	2868	2732
	PBMC	GSE62525	2130	3144
LTB and ATB	DC	GSE84344	94	123
	Mono	GSE54992	2933	2577
	PBMC	GSE62525	2155	1809

inflammatory response, GO_0002696 - positive regulation of leukocyte activation, GO_0042113 - B cell activation, GO_0001819 - positive regulation of cytokine production.

The results of GO-CC enrichment analysis showed 21 GO terms with the Top 10 terms including: GO_0060205 - cytoplasmic vesicle lumen, GO_0031983- vesicle lumen, GO_0034774- secretory granule lumen, GO_0042581 - specific granule, GO_0035580 - specific granule lumen, GO_0005766 - primary lysosome, GO_0042582 - azurophil granule, GO_1904724 - tertiary granule lumen, GO_0070820 - tertiary granule, GO_0101002 - ficolin-1-rich granule.

For the molecular function, results of GO-MP analysis showed 3 GO terms including: GO_0004869 - cysteine-type endopeptidase inhibitor activity, GO_0048029 - monosaccharide binding, GO_0038187 - pattern recognition receptor activity. According to our GO analysis, immune cells exhibited responses to *Mtb* infection at molecular level with diverse manifestations. Although the immune system was effective at suppressing the pathogen, it was unable to eliminate *Mtb* entirely. Consequently, *Mtb* would adapt and develop by restraining genes involved in the body's immune response. The finding of these genes by GO analysis would improve our knowledge about targets genes of *Mtb* that weaken human immune responses.

The KEGG pathway analysis identified various pathways involved in the biological process of interested genes. Our results mainly showed hsa04662_ B cell receptor signaling pathway, hsa04620_Toll-like receptor signaling pathway related to Immune system; hsa04932_ Non-alcoholic fatty liver disease related to Endocrine and metabolic disease; hsa05202_Transcriptional misregulation in cancer related to Cancer (Fig. 6B).

3.4. Prediction of changes in gene expression

To predict potential miRNAs and genes that may change expression

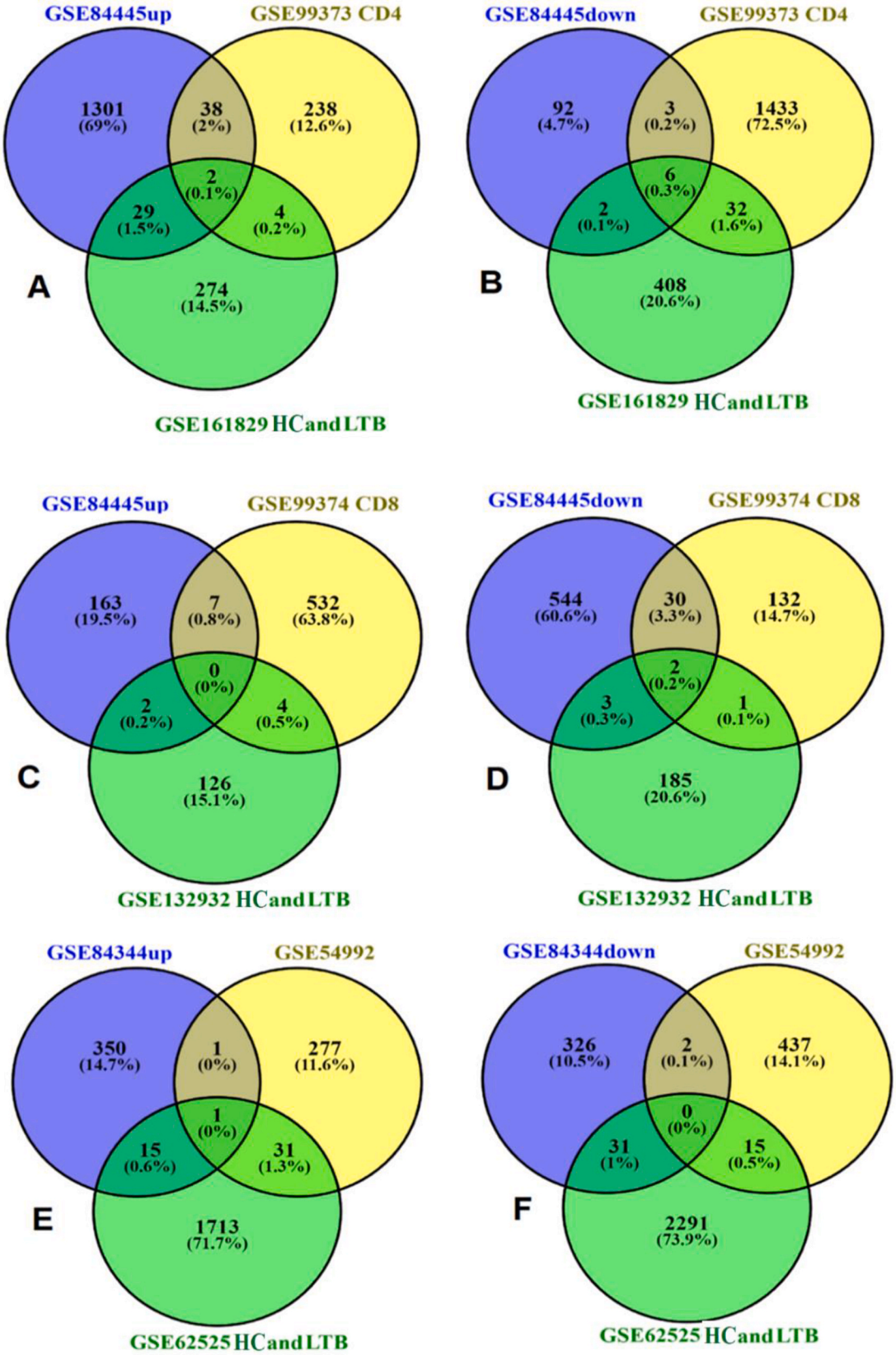

Fig. 3. Venny's analysis of datasets comparing the HC and LTB stage (A) up-regulated genes in $CD4^+$ T-cell; (B) down-regulated genes in $CD4^+$ T-cell; (C) up-regulated genes in $CD8^+$ T-cell; (D) down-regulated genes in $CD8^+$ T-cell; (E) up-regulated genes in DC, Mono, PMBC; (F) down-regulated genes in DC, Mono, PMBC.

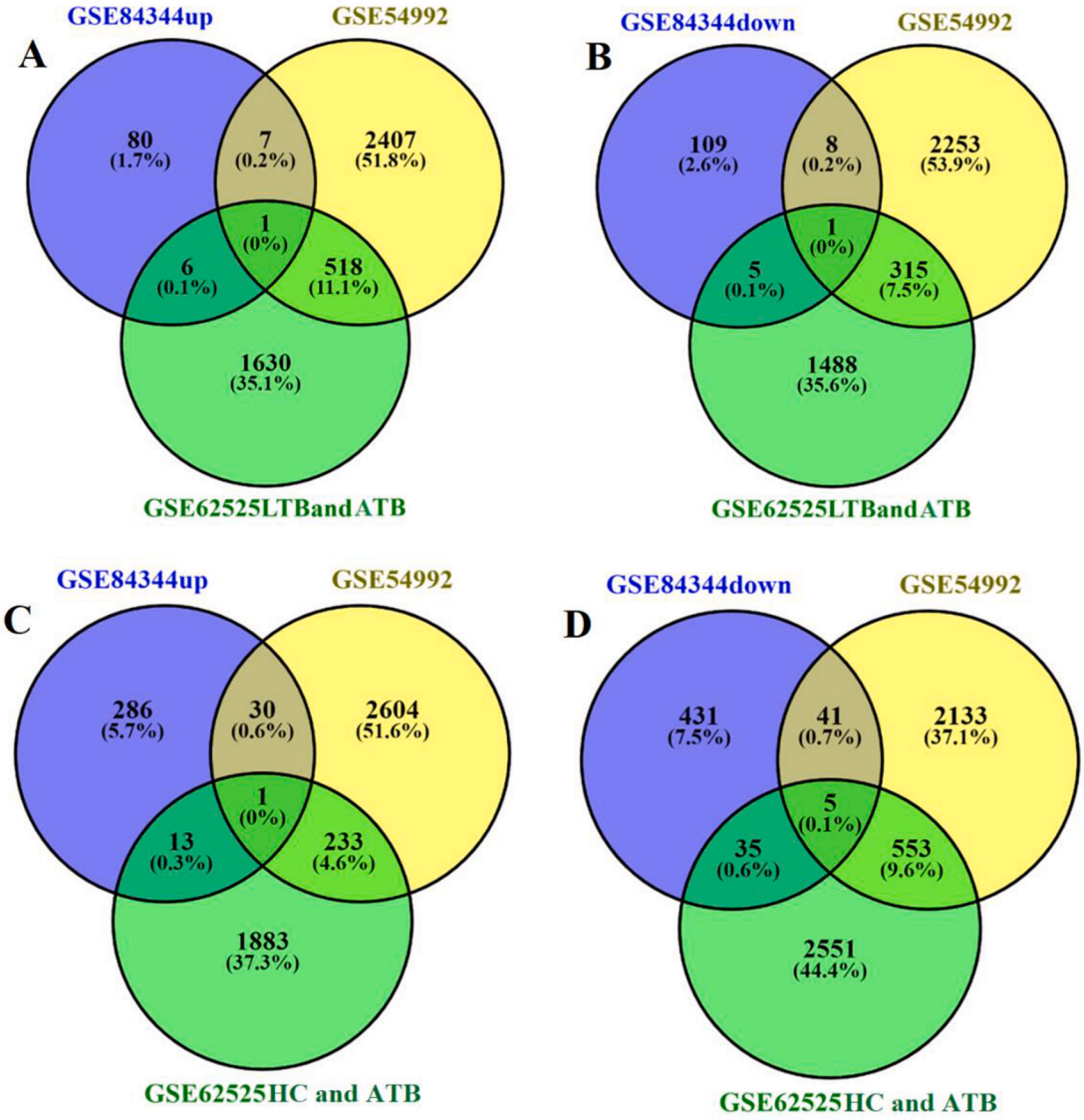

Fig. 4. Venny's analysis of datasets comparing HC, LTB and ATB stages. (A) up-regulated genes in DC, Mono, PMBC; (B) down-regulated genes in DC, Mono, PMBC; (C) up-regulated genes in DC, Mono, PMBC; (D) down-regulated genes in DC, Mono, PMBC.

in different stages of tuberculosis, we followed methodologies described in many previous studies [43–47]. We hypothesized that these predicted potential genes have certain roles in the progression of tuberculosis in humans. Therefore, we compared the altered gene expression between each stage of TB and identified a number of dysregulated genes using theVenny tool (Fig. 7).

The results describe the differential expression of each molecular marker at different stages. Although results are collected from multiple data sources, tour primary objective is to present the most promising markers, proposing them for validation in future cohort studies involving patient blood samples to confirm their diagnostic value.

3.5. Prediction of potential miRNA/gene interaction networks

Cytoscape software was useful in constructing the miRNA/gene interaction network. Simultaneously, the results of GO and KEGG analysis allowed us to identify genes involved in various cell functions and signaling pathways. A subnetwork was predicted for the potential role of molecular markers (Fig. 8).

3.6. Predicted potential miRNAs and genes

Estimation of the area under the ROC curve (area under curve, AUC) was performed to evaluate the sensitivity and specificity of most relevant miRNAs and mRNAs (section 3.6). All results displayed AUC >80 %, indicating high diagnostic accuracy of the tests and suggesting the potential of these miRNAs and mRNAs as biomarkers for TB diagnosis using blood samples (Tables 5 and 6 and Fig. 9).

Although the number of samples is small, the results obtained through bioinformatics analysis can serve as a prospective study from which to screen out new feasible molecular targets. Among the many gene targets predicted,the confirmation of AUC values > 80 % will help us focus more on important genes for cohort trials in human blood samples. This approach is expected to reduce both research time and costs for screening the expression of each specific gene target.

3.7. Prediction of potential therapeutic drugs

The DGIdb database was utilized to screen for potential anti-TB drugs targeting TB-related hub genes. IL1β was identified as a promising therapeutic target with several drug options, while no potential drugs

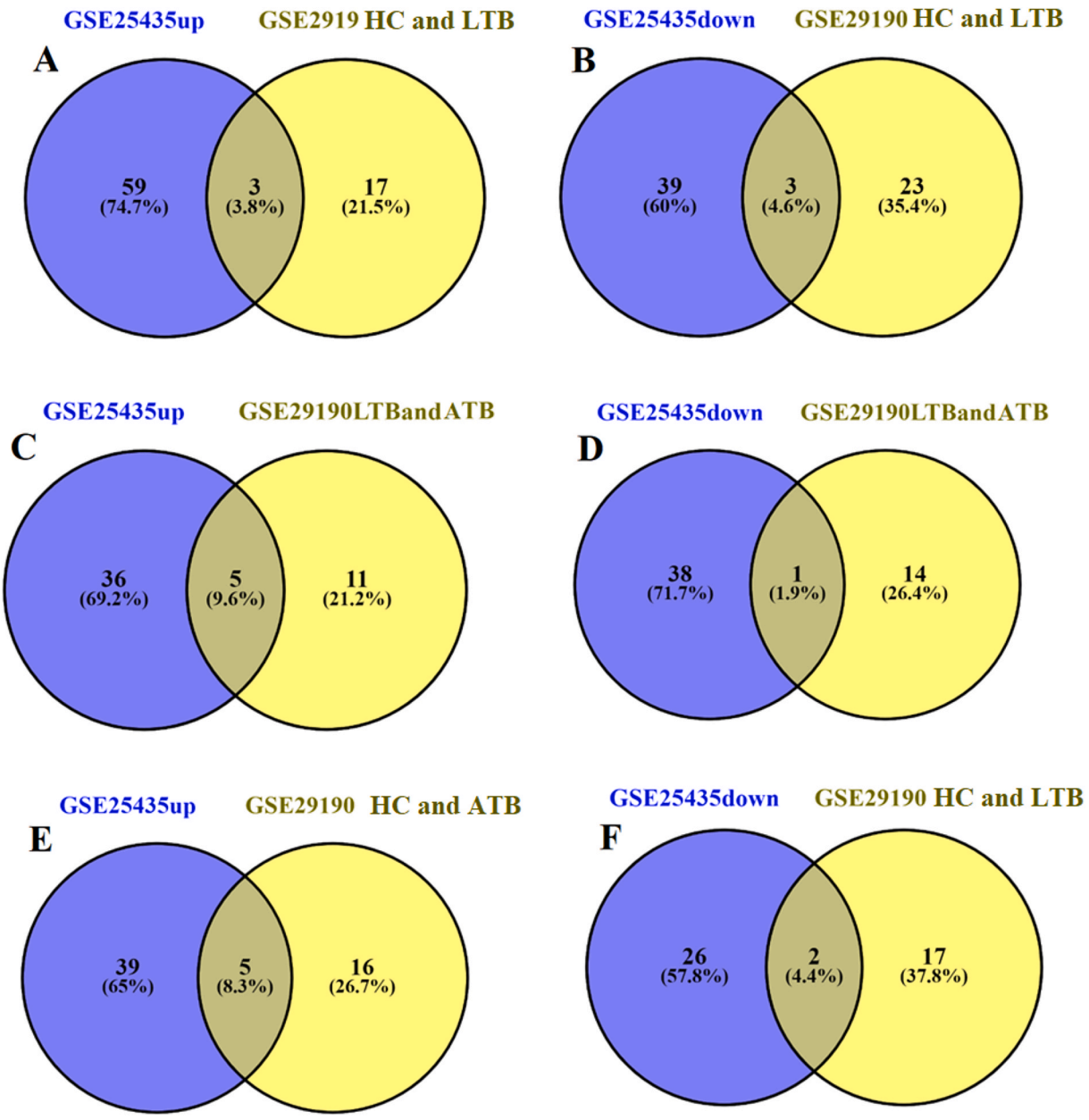

Fig. 5. Differentially expressed miRNA results were selected from overlapped datasets at different stages of disease progression. (A) up-regulated miRNA between HC and LTB; (B) down-regulated miRNA between HC and LTB; (C) up-regulated miRNA between LTB and ATB; (D) down-regulated miRNA between LTB and ATB; (E) up-regulated miRNA between HC and ATB; (F) down-regulated miRNA between HC and ATB.

Table 4
Results of differentially expressed miRNAs.

miRNAs expression	LogFC			LogFC		
	Up-regulated	GSE25435	GSE29190	Down-regulated	GSE25435	GSE29190
CT-LTB	hsa-miR-212	0.881291762	0.981251	hsa-miR-186	−1.3646	−2.01952
	hsa-miR-500	0.919911337	1.020069	hsa-miR-29a	−1.24627	−1.76636
	hsa-miR-576-5p	1.127638401	1.010948	hsa-miR-15b-5p	−0.93388	−1.84811
LTB-ATB	hsa-miR-199b-5p	1.014710884	0.751689	hsa-miR-342-5p	−0.60873	−1.31221
	hsa-miR-421	1.220392165	0.531174			
	hsa-miR-196b	1.263440049	0.738152			
	hsa-miR-144-3p	1.396353776	2.423271			
	hsa-miR-21	2.55076356	1.136446			
CT-ATB	hsa-miR-329	0.867981	0.864505	hsa-miR-150	−1.341859	−0.79451
	hsa-miR-582-5p	1.177274	2.336047	hsa-miR-186	−0.562571	−1.76088
	hsa-miR-199b-5p	1.226041	2.402682			
	hsa-miR-21	1.304821	1.178451			
	hsa-miR-500	1.316283	0.970457			

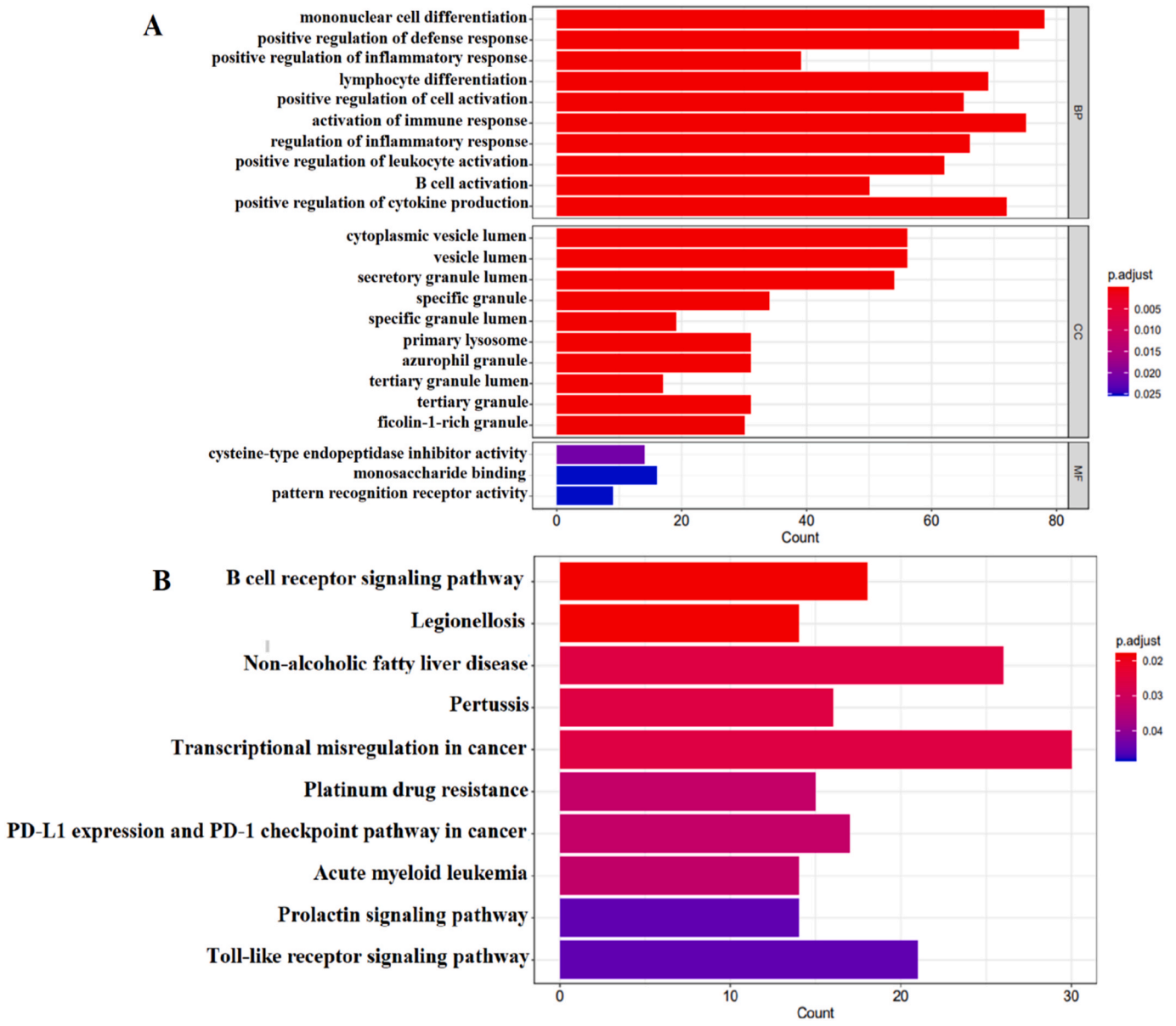

Fig. 6. GO and KEGG analysis results. (A) GO terms; (B) Signaling pathways from KEGG analysis.

were found for PLEKHG1, CLPB, DOK4, and TLR3. Our molecular docking analysis revealed several inhibitors against Human Interleukin-1 Beta, with binding affinities ranging from −4.7 to −7.9 kcal/mol (Table 7). Notably, Celastrol and Cefaclor Anhydrous showed the highest binding affinities, suggesting strong potential as inhibitors.

Celastrol showcased a strong affinity for Human Interleukin-1 Beta (IL1β), demonstrating a binding affinity of −7.9 kcal/mol. This affinity is indicative of the potential of Celastrol as a significant inhibitor of IL1β. The docking pattern analysis (Fig. 10A) revealed that Celastrol forms critical interactions with the protein, contributing to its high binding affinity and potential inhibitory activity. Celastrol forms conventional hydrogen bonds with LEU 80 and PRO 78, with distances of 2.46 Å and 2.33 Å (Fig. 10B and C), respectively. These interactions are crucial for the stability of the Celastrol- IL1β complex, indicating a specific binding mechanism that could hinder the protein's function. Additionally, a Pi-Anion interaction with GLU 25 (3.51 Å) suggests further specificity and potential for disrupting the activity of IL1β. Moreover, Celastrol engages in Pi-Alkyl interaction with PHE 133 and an Alkyl interaction with PRO 131(Fig. 10B and C), which further stabilizes the complex and contributes to the inhibitory effect. The compound also forms multiple van der Waals interactions with amino acids such as TYR 24, LEU 82, GLN 81, LEU 26, VAL 132, LYS 74, THR 79, and LYS 77, highlighting the extensive interaction at the binding site that Celastrol establishes with IL1β.

Cefaclor Anhydrous showed the highest binding affinity of −7.8 kcal/mol. This molecule demonstrated significant interaction with IL1β (Fig. 11A), indicating its potential as an inhibitor. Cefaclor formed conventional hydrogen bonds with LEU 62, GLU 64, and SER 43, which are crucial for its binding affinity. These hydrogen bonds, with distances of 2.68 Å, 2.36 Å, and 3.06 Å, respectively, suggest strong and specific interactions likely contributing to the compound's inhibitory effect (Fig. 11B and C). Additionally, a carbon-hydrogen bond with SER 05 (3.09 Å) and an alkyl interaction with PRO 91 (4.84 Å) were observed, further stabilizing the Cefaclor- IL1β complex. An amide-Pi stacked interaction with LYS 65 (3.82 Å) highlights the specificity of Cefaclor to the IL1β binding site. The presence of multiple van der Waals interactions with residues such as LEU 67, TYR 68, and others, contribute to the overall binding stability.

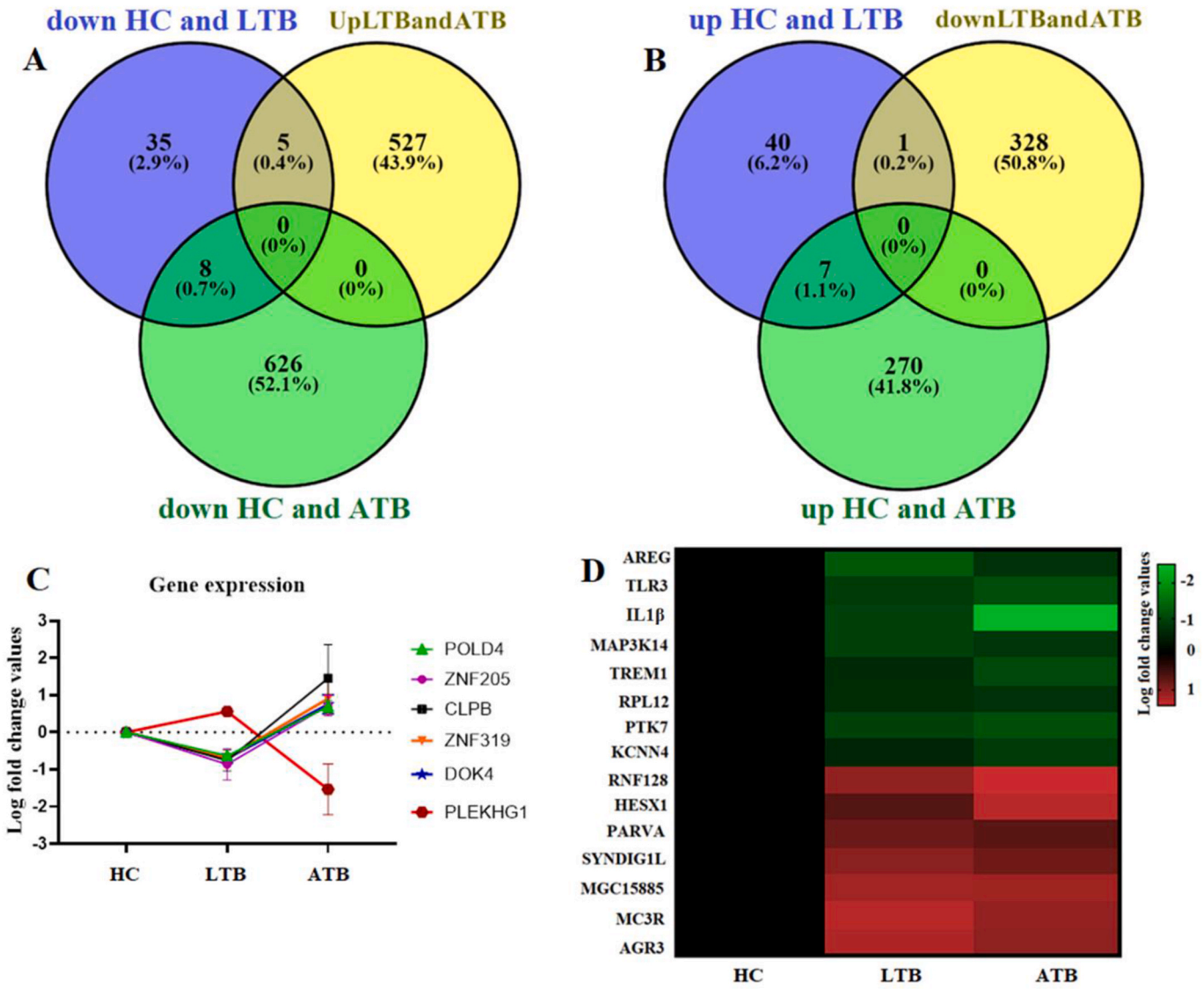

Fig. 7. Results of gene interference showing changes between stages of tuberculosis progression. (A) Data collection results from Venny tool; (B) Representation of dysregulated genes between different stages of TB progression; (C)Heatmap of genes with up-and down-regulation during the progression of tuberculosis. Green shows down-regulated genes compared to Healthy control; Red shows up-regulated genes compared to Healthy control.

3.8. MD simulation

We utilized advanced all-atoms MD simulations with OPLS4 force field parameters in the Desmond simulation software from Schrödinger LLC to analyze the structural dynamics of the top-ranked screened complexes [48].

The Root-Mean-Square Deviation (RMSD) values were calculated for 150 ns simulations to assess remdesivir's stability in complex with MPro. The protein's backbone exhibited RMSD ranging from 1.8 Å to 10 Å, averaging 2.1 Å (Fig. 12A). These values indicate the compound's overall stability during the simulation. In the IL1β-CELASTROL complex, stability was observed throughout the simulation, with minor fluctuations at 20 ns, 40 ns, 70 ns, and 130 ns attributed to rotatable bonds and different binding pocket positions. The IL1β-CEFACLOR ANHYDROUS system reached stability at 50 ns, with ligand deviations mainly observed from the start to 50 ns and at 135 ns due to rotatable bonds. The Ligand-RMSD fluctuated around 1.5 ± 9.5 Å, while the Protein-RMSD remained within 0.9–2.5 Å, showing progressive upsurge at 135–150 ns (Fig. 12B).

The observation was supported by RMSF analysis, determining significant rigid and flexible regions to assess functionality and compactness over time. In Fig. 14A1 and 14B1, atom-wise RMSF of A1 ranged from 4.1 to 7.2 Å, while L-RMSF for A2 displayed peaks within 0.8–3.0 Å, both containing 8 RBs (Fig. 13A2 and 13B2). Residue-wise RMSF of A1 showed fluctuations of 0.8–3 ± 0.5 Å, except for one higher peak, and P-RMSF for A2 ranged from less than 1–5 Å. Higher RMSF areas indicate loop/coil regions, while alpha helices/beta-strands contribute to rigidity with lower fluctuations. Green vertical bars indicate strong intermolecular ligand-receptor interactions with low fluctuations, reflecting high stability at the active site.

3.9. Interaction fraction analysis [49]

During MD simulations, all five compounds underwent analysis for the total number of receptor-ligand interactions, including hydrogen bonds, hydrophobic interactions, ionic interactions, and water bridges. These interactions were graphically depicted in Fig. 14. Specifically, the interaction fraction of IL1β with CELASTROL demonstrated the average binding percentage throughout the simulations (Fig. 14A). Eight residues, GLU_25, LYS_77, PRO_78, SER_125, ASN_128, LEU_136, GLN_141, and ASP_142, exhibited hydrogen bond occupancy below 60 %, whereas ALA_127, MET_130, and PHE_133 showed less than 20 % hydrophobic

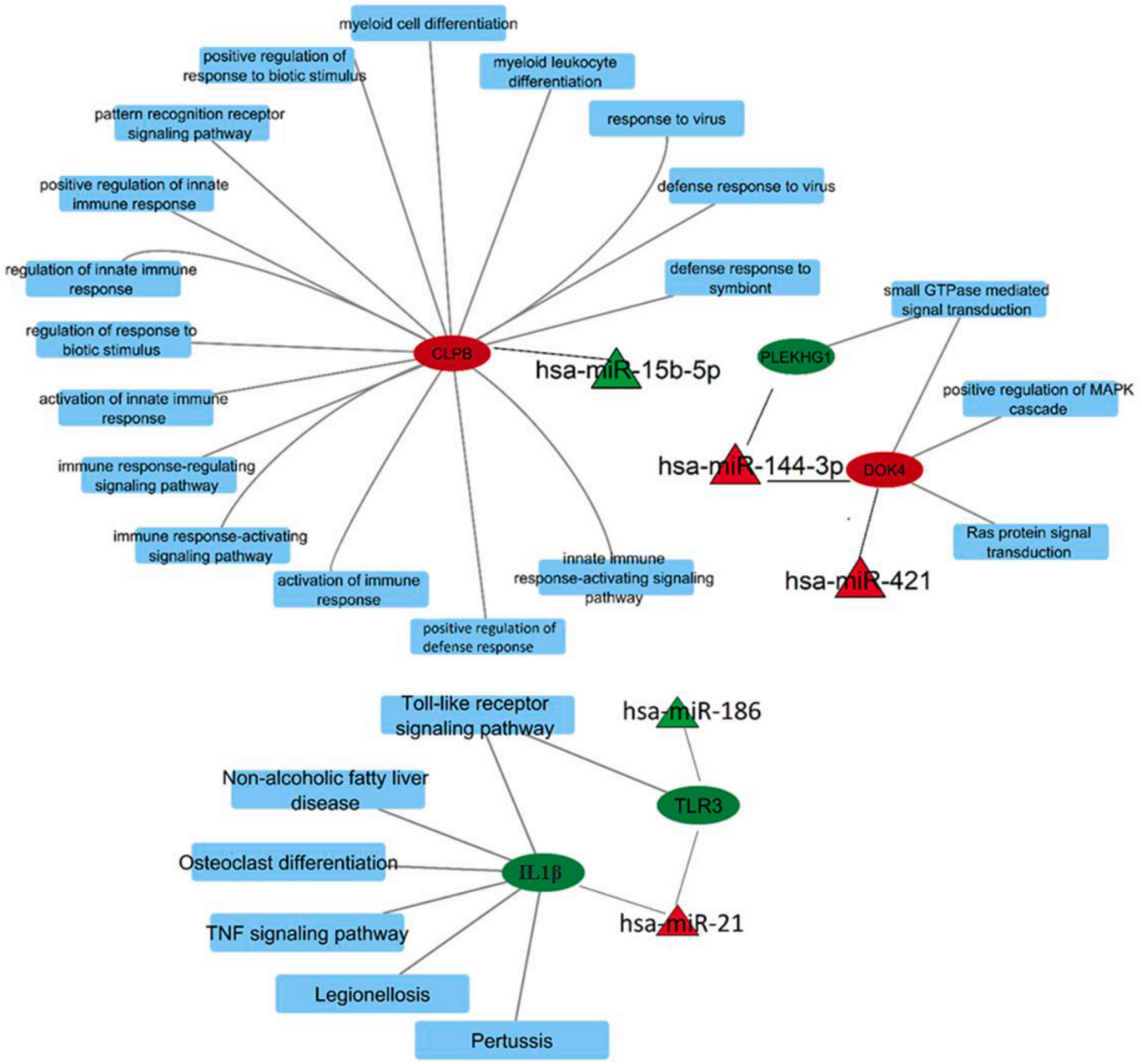

Fig. 8. Predicted role of the miRNA/gene interaction network in tuberculosis progression. The green circles represent the hub genes, the red triangles represent the miRNAs, and the blue shapes represent the pathways.

Table 5
Expression of miRNAs in each data set.

miRNA-ID	Comparison	LogFC	
		GSE25435	GSE29190
hsa-miR-15b-5p	HC and LTB	−0.93388	−1.84811
hsa-miR-186	HC and LTB	−1.3646	−2.01952
	HC and ATB	−0.562571	−1.76088
hsa-miR-21	HC and ATB	1.304821	1.178451
	LTB and ATB	2.55076356	1.136446
hsa-miR-144-3p	LTB and ATB	1.396353776	2.423271
hsa-miR-421	LTB and ATB	1.220392165	0.531174

Table 6
Gene expression in each data set.

GENE-ID	Comparison	LogFC		
		GSE84344	GSE54992	GSE62525
PLEKHG1	HC and LTB		0.625372	0.500268
	LTB and ATB		−2.0188	−1.05129
	HC and ATB		−1.39343	−0.55102
CLPB	HC and LTB		−0.96071	−0.55209
	LTB and ATB		2.093495	0.809109
DOK4	HC and LTB		−0.61668	−0.78776
	LTB and ATB		0.932366	0.572895
IL1β	HC and LTB	−1.10844		−0.8625
	HC and ATB	−0.90356	−4.15702	
TLR3	HC and ATB	−1.09821		−1.149857556
	HC and LTB	−1.11752		−0.69415

bond occupancy. Eight residues, GLU_25, LYS_27, LYS_74, ASP_75, ASP_76, LYS_77, PRO_78. THR_79, LEU_80, SER_125, GLU_128, ASN_129, VAL_132, LEU_134, GLY_139, and GLN_141, demonstrated the

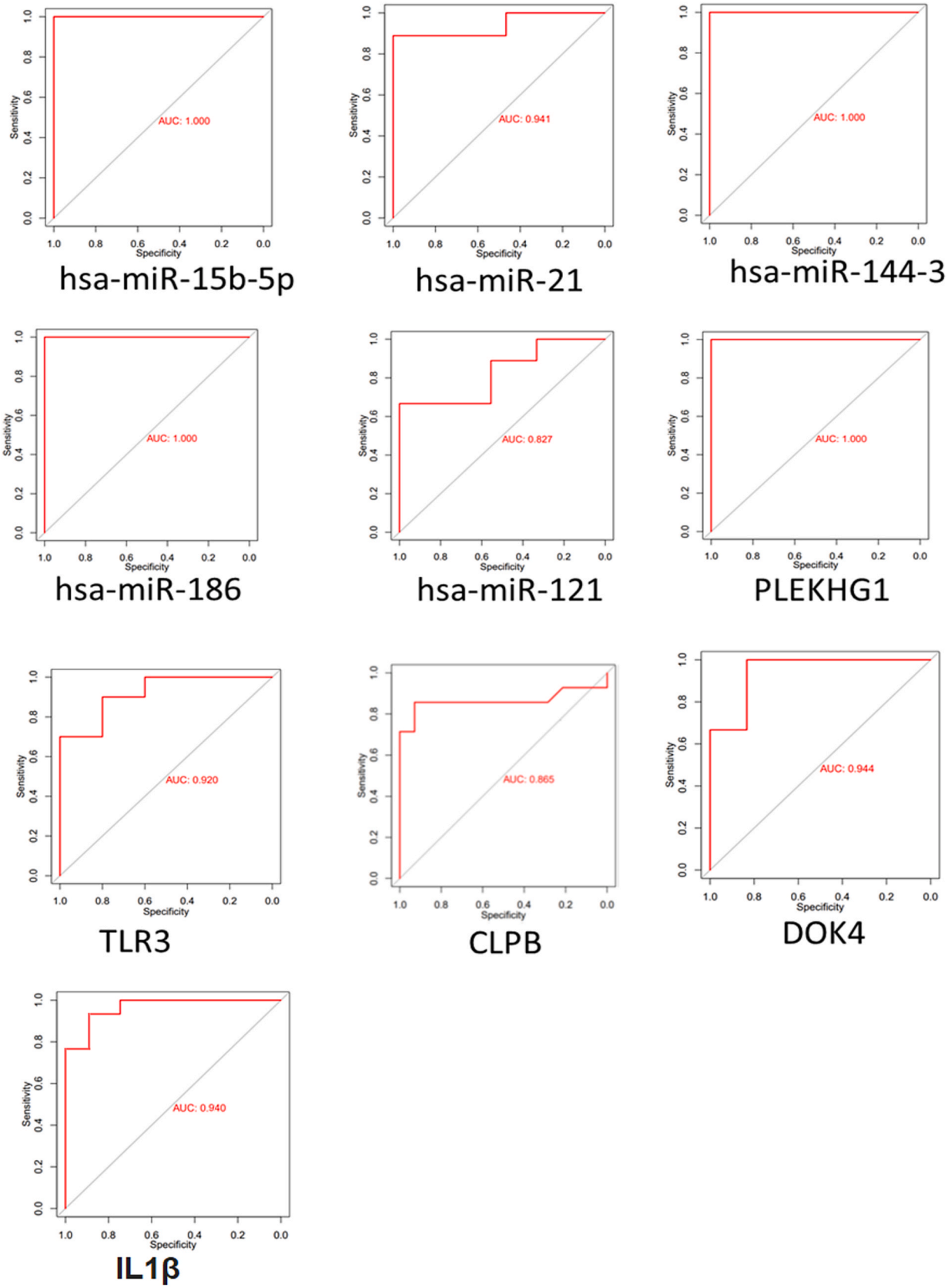

Fig. 9. Area under the curve (AUC) analysis of relevant miRNAs and mRNAs.

Table 7
Molecular docking results of potential inhibitors on Human Interleukin-1 Beta.

s. NO	Compound name	Binding affinity (kcal/mol)
1.	ETIDRONIC ACID	−5.1
2.	RESVERATROL	−6.4
3.	IBUDILAST	−5.5
4.	MELATONIN	−5.7
5.	CYTARABINE	−6.5
6.	NIMUSTINE	−6.4
7.	PENTOXIFYLLINE	−5.9
8.	RISEDRONIC ACID	−5.8
9.	TILUDRONIC ACID	−5.8
10.	ACITRETIN	−7
11.	PENTAMIDINE	−5.7
12.	OFLOXACIN	−7.1
13.	CEFACLOR ANHYDROUS	−7.8
14.	DIACETYLRHEIN	−7
15.	LANSOPRAZOLE	−7.1
16.	MAFOSFAMIDE	−4.7
17.	BECLOMETHASONE	−7.6
18.	HYDROCORTISONE BUTYRATE	−5.9
19.	FLUTICASONE	−6.9
20.	PRAVASTATIN	−5.7
21.	CELASTROL	−7.9
22.	VERAPAMIL	−5.4
23.	NICARDIPINE	−7.1
24.	RALOXIFENE	−7.6

important role of the water bridge interaction with fluspirilene. The ASP_142 residue exhibited an ionic interaction and was predicted through MD simulations and docking analysis to establish a hydrogen bond (Fig. 14A). Interaction fraction analysis of IL1β with CEFACLOR ANHYDROUS showed hydrogen bond occupancies of less than 65 % with VAL_3, SER_5, ASN_7, LEU_62, LYS_63, GLU_64, LYS_65, ASN_66, PRO_87, and TYR_90 (Fig. 14B). No ionic interactions were observed in the complex, while all bonds, except for the water bridge, played significant roles, as depicted in Fig. 14B furthermore, Calculations of both complxes of each frame along the x-axis revealed diverse independent interactions with the ligand through heatmap throughout their respective trajectories (Fig. 15). Interaction fraction analysis revealed additional interactions during MD simulations compared to docking results. These additional interactions notably contributed to the establishment of strong interaction patterns within the IL1β pocket site. This intricate interplay influences protein stability, with rigid regions showing lower RMSD compared to coils and loops. Hydrogen bonds, constituting the majority of impactful ligand-protein interactions, are highlighted in our compelling visualization (Figs. 14–15).

3.10. Ligand torsion profile

Fig. 10 presents Ligand Torsion Profiles during the 100 ns Molecular Dynamics (MD) simulation of interactions of IL1β with Celastrol and Cefaclor Anhydrous (a), Rank 1 indirubin derivative (b). The torsion plot in Fig. 16AB illustrates the rotational behavior of each ligand's rotatable bond (RB) during the simulation, color-coded for clarity. A 2D ligand schematic accompanies each plot, aiding visualization. In each subsection of Fig. 16AB, the combined use of radial plots and bar graphs provides insights into the ligand's torsional dynamics throughout the simulation. The radial plot visualizes the torsional evolution, expanding from the simulation's onset at the center. Bar graphs complement this data, showing torsion probability density. If available, combined torsional potential data is depicted in kilocalories per mole (kcal/mol) on the left Y-axis. This information is crucial for understanding potential conformational strains a ligand may experience when bound to a protein. Recognizing these nuances is vital for identifying potential challenges in drug design; for instance, significant torsional stress may suggest difficulties in maintaining the preferred conformation within the protein, impacting inhibitory potency. In conclusion, the Ligand Torsion Profiles in Fig. 11 enhance our comprehension of the ligands' dynamics within the IL1β binding site during the MD simulation. This detailed insight improves our understanding of these compounds' potential as IL1β inhibitors. By mapping out the ligands' conformational changes throughout the simulation, we gain a better understanding of their flexibility and ability to maintain a suitable conformation for effective IL1β binding.

3.11. Ligand properties

In the subsequent analysis, depicted in Fig. 17, we delved into the ligand's distinctive attributes, including RMSD, radius of gyration (rGyr), intramolecular hydrogen bonds (intraHB), molecular surface area (MolSA), solvent accessible surface area (SASA), and polar surface area (PSA). The RMSD reflects structural stability and ligand fluctuations, vital for assessing simulation reliability, in first complex (IL1β-Celastrol) values ranged from 0.10 Å to 0.75 Å, and its balance was approximately 0.65 Å while in second complex (IL1β-Cefaclor Anhydrous) ranged from 0.00 Å to 2.4 Å, and its balance was approximately 0.85. rGyr measures ligand compactness, with stable values indicating structural maintenance. IntraHB, monitoring internal hydrogen bonds, indicates structural integrity, with higher counts suggesting rigidity, The rGyr considerably varied in the ligand up until 150 ns of the simulation period in both complexes and ranged from 4.2 $Å^2$ to 4.50 $Å^2$ in frist

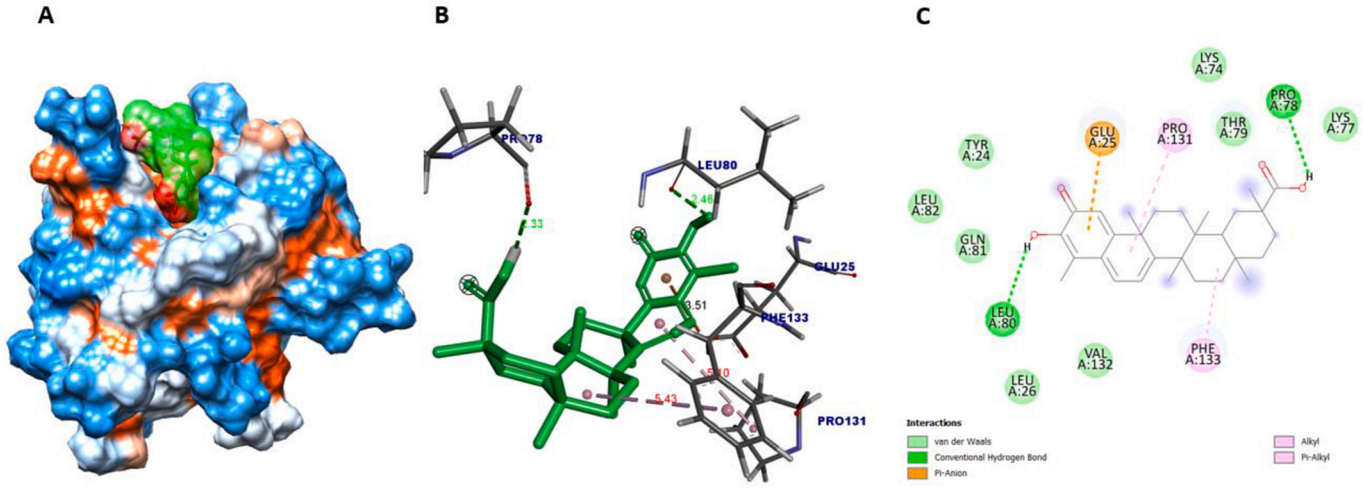

Fig. 10. Intermolecular interactions between ligand (CELASTROL) and receptor (HUMAN INTERLEUKIN-1 BETA) **A**: Binding position of Celastrol on hydrophobic surface of IL1β. **B**: Intermolecular interactions with nearby amino-acids **C**: Two-dimensional interactions between ligand and receptor.

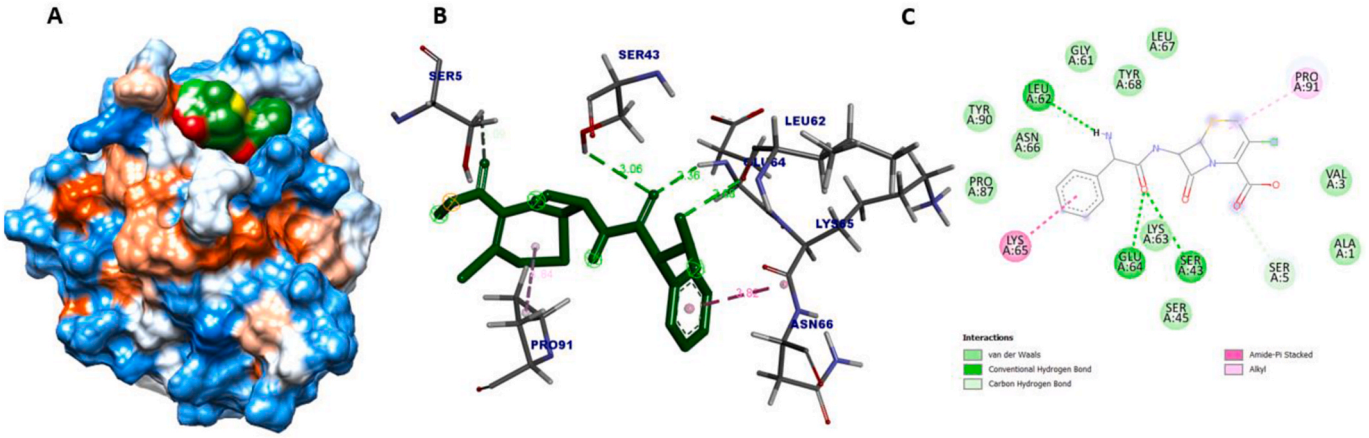

Fig. 11. Intermolecular interactions between ligand (CEFACLOR) and receptor (HUMAN INTERLEUKIN-1 BETA) A: Binding position of Cefaclor on hydrophobic surface of IL1β. B: Intermolecular interactions with nearby amino-acids C: Two-dimensional interactions between ligand and receptor.

complex while in second it was 3.2 Å^2 to 4.00 Å^2. MolSA provides insights into overall shape and size, indicating potential conformational changes, MolSA values for the ligands ranged from 380 Å^2 to 388 Å^2 while in second complex it 270 Å^2 to 300 Å^2. SASA and PSA are crucial for understanding ligand-environment interactions. SASA offers insight into the ligand's solvent-exposed surface area, indicating potential solvent interaction shifts. The SASA of the *both* ligand complex noted as stabilized in MD simulation. It ranged from 100 Å^2 to 300 Å^2 and reached equilibrium at approximately 289 Å^{2}in first complex while in second complex it showed some fluctuation however still stabilized at 400 Å^2. while PSA is crucial for understanding solubility and permeability, often indicating membrane traversal capability or bloodstream solubility dynamics, The PSA values of the ligand varied from 152 Å^2 to 162 Å^2 in first complex, while in second it was 140 Å^2 to 225 Å^2. These parameters collectively depict the ligand's dynamic behavior during simulation, aligning with core manuscript findings and providing crucial insights for drug design initiatives.

3.12. Principal component analysis (PCA)

The PCA is a vital method for reducing dimensionality in complex datasets, aiming to preserve essential information. This technique extracts a set of linear combinations, known as principal components, from the data. These components are carefully constructed to capture the most significant variability within the dataset, providing a comprehensive representation of its inherent patterns and trends. Three key principal components, named PC1, PC2, and PC3, were retrieved from MD simulation trajectories, focusing on the maximum amount of data for PCA analysis. In case of IL1β with Celastrol complex. The stability of the first 20 modes of motion is depicted in Fig. 18, showing eigenvalues alongside eigenvector data for the protein. These eigenvalues represent fluctuations in hyperspace eigenvectors, where complex eigenvalues indicate the overall flexibility of the target protein in simulation analyses. The top five eigenvectors in the studied schemes demonstrate prominent movements, with larger eigenvalues compared to others. All observed changes are graphically represented in three principal components (PC1, PC2, and PC3). PC1 clusters exhibit the greatest inconsistency (23.18 %), followed by PC2 (9.99 %) and PC3 with the lowest inconsistency (9.2 %) (Fig. 18A). PC3, due to its lower inconsistency, demonstrates a more condensed structure compared to PC1 and PC2, indicating enhanced stability in the protein-ligand binding complex. Analysis of conformational variations across groups within the PC subspace shows distinct mobility levels—blue denotes significant movement, white represents intermediate, and red indicates lower flexibility (Fig. 18B).

PCA analysis of IL1β with Cefaclor Anhydrous complexes was conducted, revealing PC1 clusters with the highest inconsistency (17.53 %), followed by PC2 (13.53 %) and PC3 with the lowest inconsistency (7.76 %) (Fig. 16A). PC3 exhibited a more condensed structure compared to PC1 and PC2 due to its lower inconsistency, indicating enhanced stability in the protein-ligand binding complex. Conformational variations across groups within the PC subspace displayed distinct mobility levels—blue representing significant movement, white indicating intermediate, and red suggesting lower flexibility (Fig. 19B).

3.13. MM-GBSA

The MMGBSA method was utilized to assess the binding energy of ligands to proteins, with the top compounds Celastrol and Cefaclor Anhydrous showing the lowest binding energies of 7.9 kcal/mol and −7.8 kcal/mol with IL1β. This method reveals the dynamic interplay of non-bonded interactions, encompassing Coulombic forces and van der Waals energies, which shape the complex binding landscape. Detailed results in Tables 8 and 9 highlight the significant influence of G_{bind}Lipo, G_{bind}vdW, and G_{bind}Coulomb energies on the average binding energy across various interactions, providing valuable molecular insights into protein-ligand dynamics while whole details are provided in (Tables S1–S2).

The G_{bind}SolvGB and G_{bind} Covalent energies were found to play minor roles in the overall binding energies, with both complexes demonstrating remarkable stability. This was primarily due to strong hydrogen bonds formed with amino acid residues, as evidenced by their impactful $G_{bind}H_{bond}$ interaction values. These findings provide strong validation for the binding energy derived from docking data, further supported by MM-GBSA calculations based on dynamic MD simulation trajectories.

4. Discussion

Tuberculosis (TB), caused by *Mtb*, is a contagious chronic disease primarily affecting the lungs, leading to severe hemoptysis and fever [50,51]. Recent studies have highlighted the crucial role of macrophage dysregulation in the onset, progression, and prognosis of TB [52]. Investigating immune response-related genes is pivotal in uncovering the mechanism undelying TB susceptibility [53]. In this pilot study mRNA profiles from TB and normal blood samples were analyzed, leading to the identification of 6 hub genes within the M1 macrophage infiltration model. Notably, four of these hub genes emerged as reliable candidate biomarkers with markedly elevated levels in TB samples. The study also predicted 24 small molecules as potential theurapeutic agents targeting the biological mechanisms of tuberculosis. Enrichment analysis revealed a strong association between the identified hub genes and

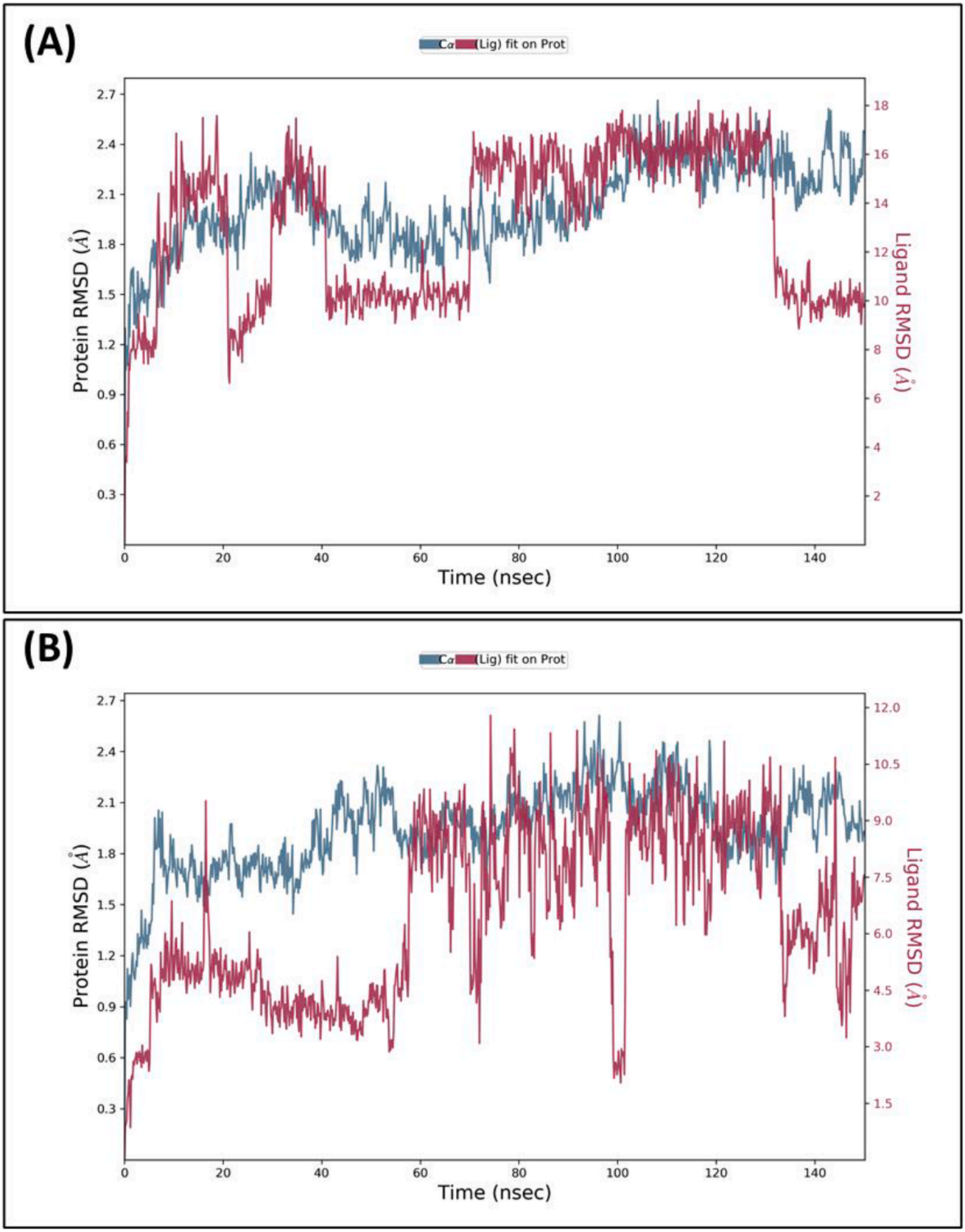

Fig. 12. The root-mean-square deviation (RMSD) of IL1β (A) with CELASTROL (6LU7), and (B) with CEFACLOR ANHYDROUS.

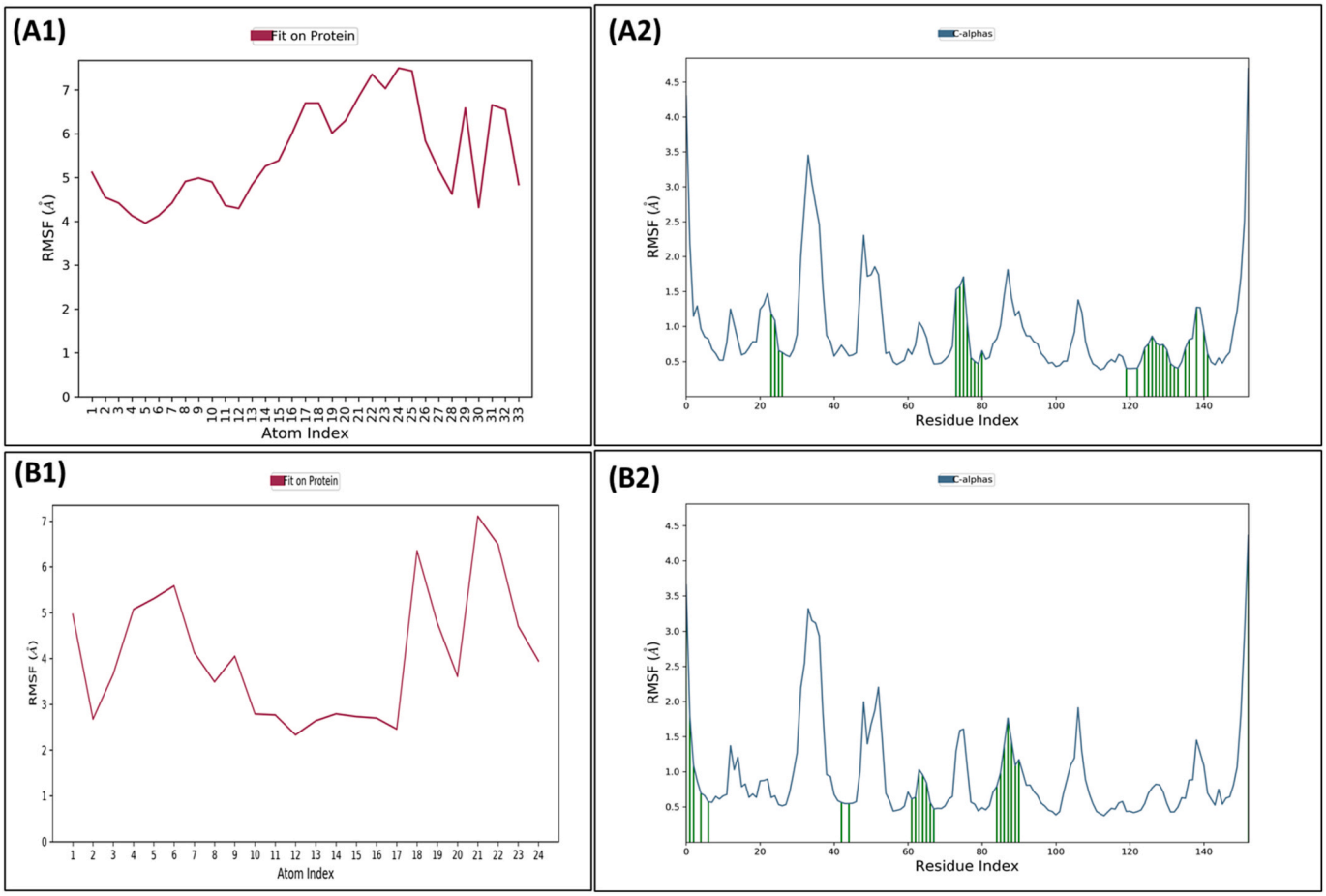

Fig. 13. (A1) Atom-wise RMSF of A1 compound and (B1) A2 in contact with target protein IL1β (red color) while (A2) and (B2) shows Residue-wise RMSF of protein in contact with A1 (upper panel) and A2 (lower panel).

the immune responses to tuberculosis. Specifically, PLEKHG1, CLPB, DOK4, IL1β, and TLR3 emerged as consistent candidate key genes which were common between differentially expressed genes (DEGs) and hub genes. KEGG analysis further revealed molecular pathways associated with latent tuberculosis. This study identified the downregulated genes, IL1β and TLR3, as miR-21 targets in these pathways. Hackett and colleagues confirmed that specific control of glycolysis in *Mtb*-infected cells occurs via the regulation of miR-21. Among these, the increase of glucose metabolism through glycolysis has been proven to promote macrophage activation by providing a rapid source of ATP within the cell, as well as increasing the levels of biosynthetic precursors required for inflammatory response. Moreover, *Mtb* replication in macrophages is promoted by suppressing metabolic reprogramming and associated IL1β production through miR-21 to ensure survival and replication [54]. The discovery of miR-21's role in new mRNA targets during *Mtb* infection highlights the significance of immunometabolic response in host defense. Specifically, miR-21's regulation of IL1β, a key cytokine, aligns with findings from previous leprosy research [55]. Several studies have indicated that multidrug-resistant *Mtb* strains restrict IL1β production by inhibiting metabolic reprogramming [56]. In addition, Keegan and colleagues proposed a mechanism by which TLR3 cooperates with TLR8 in Th1 pathway induction, involving IFN and downstream gene activation, culminating in IL-12p70 production that essential for initiating Th1 responses, a key component of the host defense mechanism [57]. TLR3 has also been reported to directly activate NK cells [58]. This data is highly relevant in our prediction of the miRNA/gene interaction network, suggesting that the selected hub genes and miRNAs may play a critical role in LTB and may interact with each other. They could serve as potential candidates for early diagnosis or prognosis of LTB. The downregulation of IL1β and TLR3 stands out as independent biomarkers intricately tied to the progression of *Mtb* infection, providing insights into their roles within immune responses and activity pathways. This study enhances our understanding of their molecular mechanisms, paving the way for their potential application as valuable diagnostic tools for tuberculosis.

Our analysis suggests that genes implicated in the B cell receptor signaling pathway are potentially crucial in LTB. This finding aligns with prior research, as Stewart et al. highlighted the previously underappreciated role of B cells in the immune response to *Mtb* infection. Although T cells and macrophages were traditionally emphasized, recent evidence underscores the active involvement of B cells during the acute phase, where they enhance phagocytosis as well as cytokine and antibody release [59]. Lee et al. identified two pathways responsible for the secretion of IL1β by monocytes and macrophages: the inflammasome pathway and the NF-κB pathway. NF-κB is recognized for its role in regulating and promoting the secretion of various cytokines, including IL1β and TNF-α. Inflammasomes are complexes made up of multiple proteins from the innate immune system that trigger inflammatory responses through toll-like receptors (TLRs) and nod-like receptors (NLRs), which interact with several adaptor proteins leading to caspase-1 activation and the release of proinflammatory cytokines such as IL1β and IL-18 [60,61]. IL1β is crucial in mediating inflammation and the immune response in hosts by influencing the function of different cells, both individually and alongside other cytokines [62]. The production and release of IL1β are carefully controlled at both transcriptional and secretory levels. Multiple proteins, including pyrin, PI-9 (an inhibitor of caspase-1), and certain CARD-containing proteins regulate IL1β production by interfering with caspase-1 recruitment or

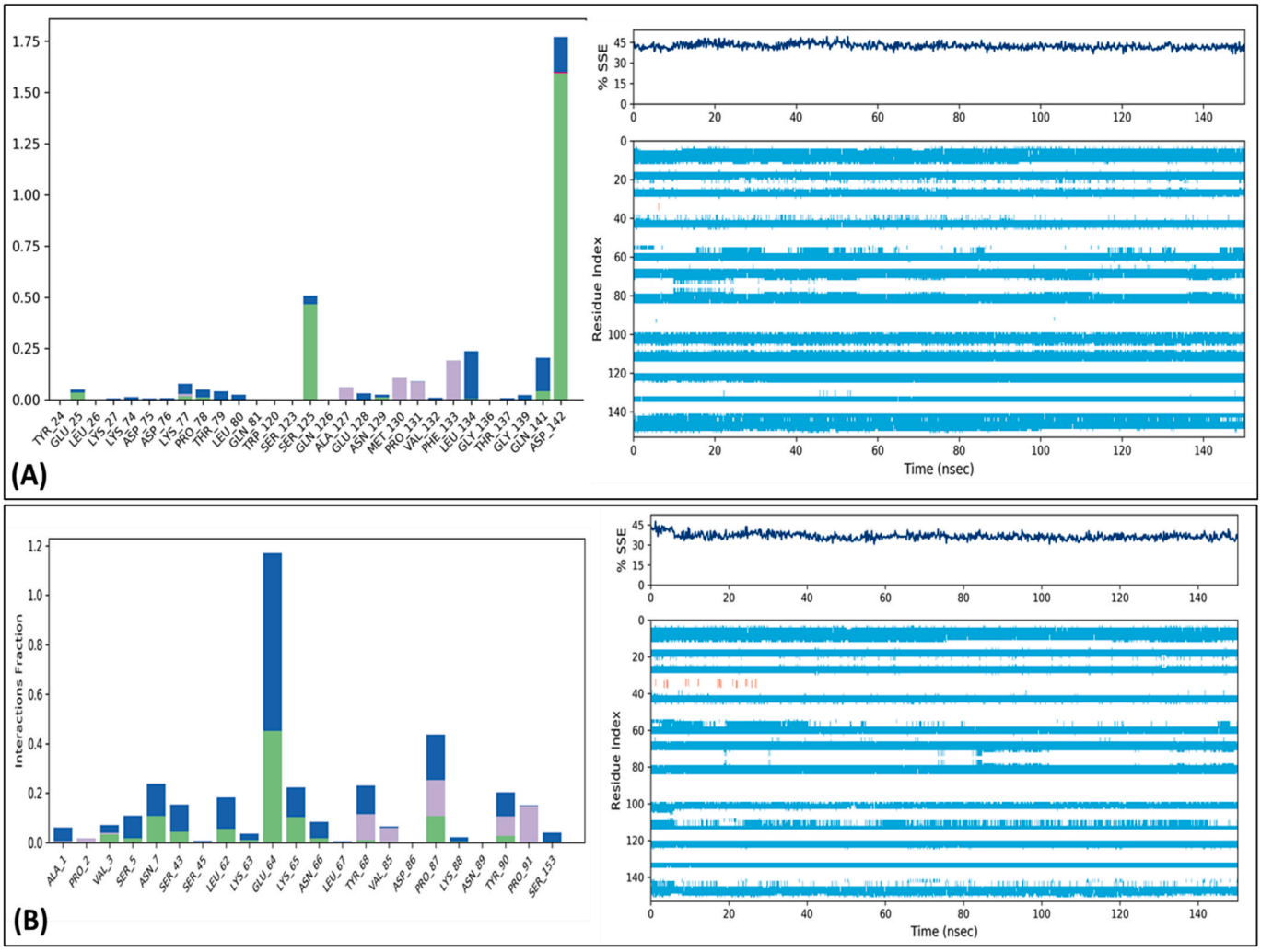

Fig. 14. Graphical representation of interaction fraction analysis: (A) Interaction between IL1β and CELASTROL, Elements of protein 2D structure are discrete across protein and ligand complexes with respect to thier residue index. (B) Interaction between IL1β and CEFACLOR ANHYDROUS, The elements of protein 2D structure are discrete across protein and ligand complexes with respect to their residue index.

neutralizing its activity directly. IL1β exerts its effects through specific binding to cell surface receptors—IL-1RI and IL-1RII [63]. Similar to mature IL-18, active IL1β is produced following the proteolytic cleavage of its precursor by caspase-1, which is activated by the inflammasome. Mature IL1β serves vital homeostatic roles and is involved in initiating antimicrobial immunity by inducing TNF-α and IL-6 release and polarizing the Th17 response. This enhances protective mucosal defense through the secretion of IL-17 and IL-22 [64,65]. The importance of IL1β in countering *Mycobacterium tuberculosis* (M.tb) has been demonstrated by findings that IL1β or IL-1R knockout mice displayed increased susceptibility to TB, with higher mortality rates and greater bacterial loads in their lungs [66]. Furthermore, antigen-specific IL1β can serve as a biomarker for distinguishing between pulmonary TB and LTB. Notably, elevated levels of IL1β and TNF-α were detected in patients with active TB compared to contacts and uninfected controls when measuring cytokines in supernatants from QFT tubes [67]. Our results enhance the understanding of TB immunology and suggest that IL1β may represent a novel immune cell signature biomarker that differentiates LTB cases from active TB patients.

In this study, molecular docking revealed Celastrol and Cefaclor Anhydrous could have potential therapeutic role in TB by targeting IL1β, supporting its use as a drug candidate. Additionally, the results indicated that celastrol, known for its anti-inflammatory, antiviral, immune regulatory, and anti-tumor properties, shows promise for further investigation [68–71]. Celastrol low toxicity, multitargeting capability, and broad-spectrum activity have garnered significant interest as an anticancer therapy, particularly in lung cancer [72], colorectal cancer [73], liver cancer [74], gastric cancer [75] hematological malignancies [76], renal carcinoma [77], prostate cancer [78], bone tumor [79], breast cancer [80], cervical cancer [81], brain tumor [82], and ovarian cancer [83]. Furthermore, Celastrol inhibits rheumatoid arthritis by inducing autophagy via inhibition of the PI3K/AKT/mTOR signaling pathway suggesting [69]. Celastrol may play a beneficial role in TB. In this study, drug analysis revealed Celastrol and Cefaclor Anhydrous as potential for developing anti-TB therapeutic agents through binding to IL1β, suggesting significant implications for therapeutic interventions in LTB. Cefaclor Anhydrous, a second-generation cephalosporin, inhibits bacterial cell wall synthesis similarly to penicillins. Demonstrating activity against both gram + ve and gram -ve bacteria, this beta-lactam antibiotic has been found effective against 73.6 % of *E. coli* isolates in children from various clinical specimens in 2009 [84,85]. These findings suggest potential for cefaclor in combating bacteria associated with TB. However, the precise mechanism of action of Celastrol and Cefaclor Anhydrous requires further research.

Modern drug discovery leverages computational studies such as molecular docking, MD simulations, MM-GBSA, and PCA analysis to elucidate drug-protein interactions, binding strengths, dynamics, and overall drug properties, enhancing design optimization [86–88]. By

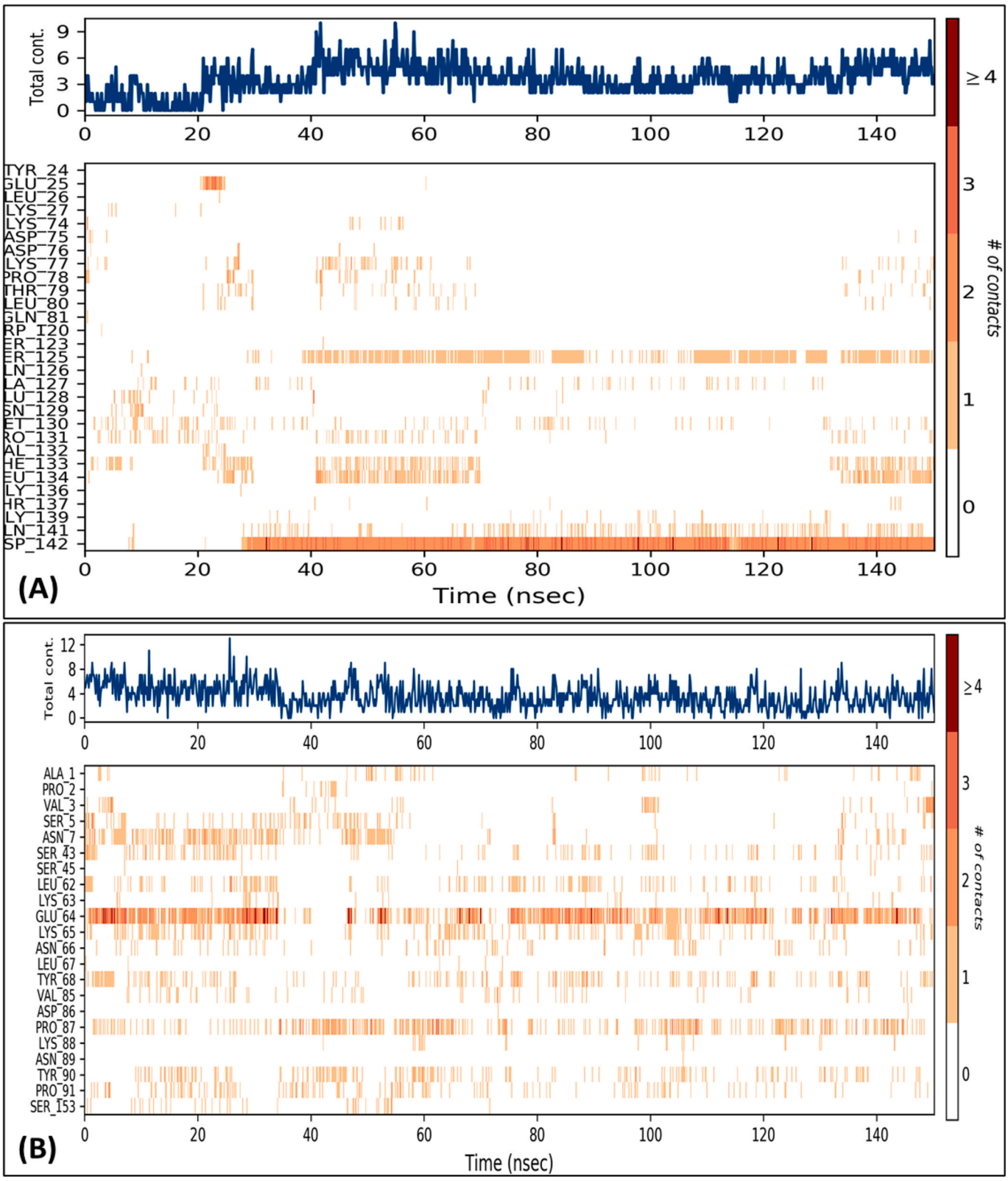

Fig. 15. illustrates the protein-ligand contact heatmap for IL1β with Celastrol (A) and IL1β with Cefaclor Anhydrous (B) throughout their respective trajectories.

focusing on IL1β, we aimed to unravel the interaction nuances of indirubin and indigo derivatives, augmenting existing anticancer activity data [89–95]. Real-life complexities may not always align with predictions, with variables like dosage and individual susceptibilities affecting hepatotoxicity [89]. Despite these challenges, our research identifies 2 structures with potential for developing leading compounds towards IL1β inhibitor candidates. Celastrol and Cefaclor Anhydrous show better intermolecular interactions with IL1β, scored by the most negative docking energy (Table 7). However, the MD simulations result show high fluctuation of both these two compounds at binding site

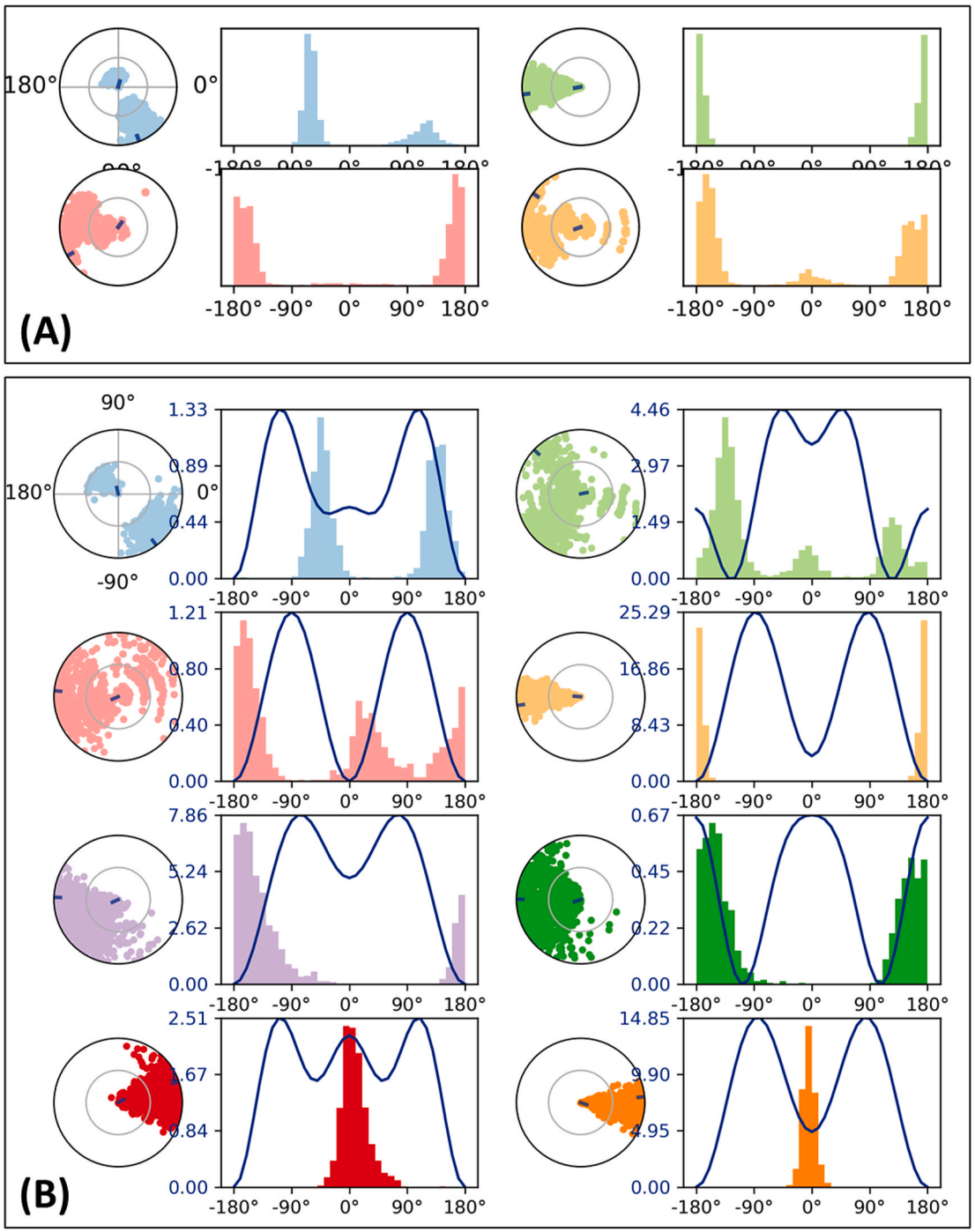

Fig. 16. Ligand Torsion Profile for (**a**) IL1β with Celastrol (**b**) IL1β with Cefaclor Anhydrous during 150 ns MD simulation run.

(Figs. 12 and 13). Despite of that, the interaction fraction analysis in Fig. 14 still indicate that, those ligands keep interacting with key amino acids which may involed in to the bioactivities of IL1β. These fluctuations highlight that the current ligand structures may require further refinement to optimize their interactions and stability. Therefore, future research should focus on improving the molecular design of these compounds to reduce structural variability and enhance binding stability. To support this argument, additional analyses such as RMSF (Fig. 13), radius of gyration and hydrogen bond occupancy has been performed (Figs. 15 and 17) to further elucidate the flexible regions and stability of the complex under different simulation conditions. Combining these results with PCA data can provide deeper insights into the major components influencing the stability of the protein-ligand complex, guiding the design of more stable ligand derivatives.

Despite the comprehensive collection of study populations from various high-throughput sequencing data sources, certain limitations must be considered. The HC/LTB/ATB classifications could be more likely the different outcome in individuals after exposure to Mtb rather than disease progression stages. Nonetheless, GO and KEGG prediction analyses showed that the gene targets identified are indeed involved in the cellular and biological processes associated with tuberculosis, further strengthening our hypothesis about the potential importance of these predicted genes. This findings provides a theoretical basis for us to continue official tests. Certain potential genes identified with differential expressions were absent in the miRNA/mRNA interaction network, possibly due to limitations within the GSE datasets, resulting in gaps in

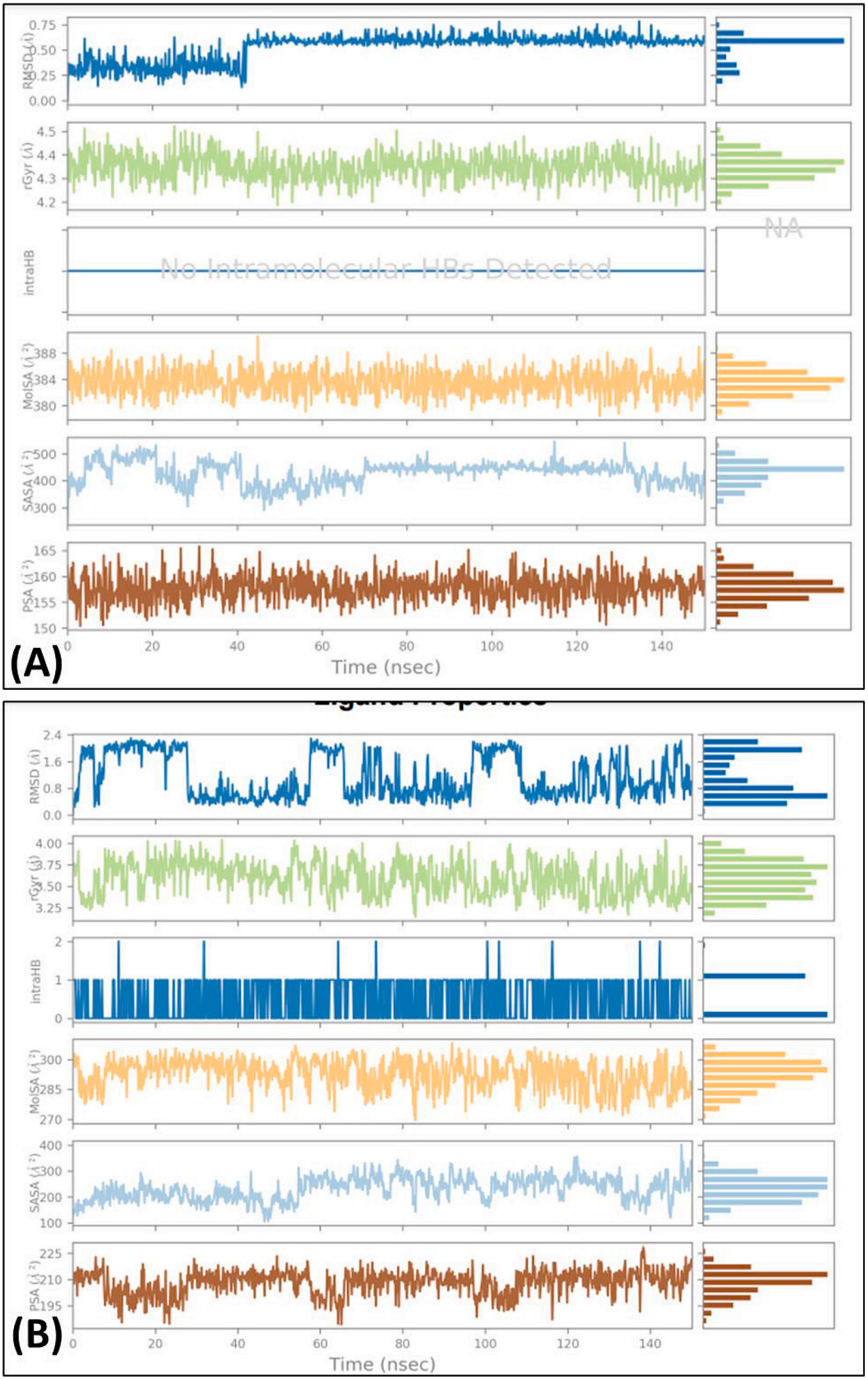

Figuer 17. Ligand properties like Radius of Gyration (rGyr), intramolecular H bonds (intraHB), Molecular Surface Area (MolSA), Solvent-Accessible Surface Area (SASA) and Polar Surface Area (PSA) for IL1β with Celastrol (**b**) IL1β with Cefaclor Anhydrous.

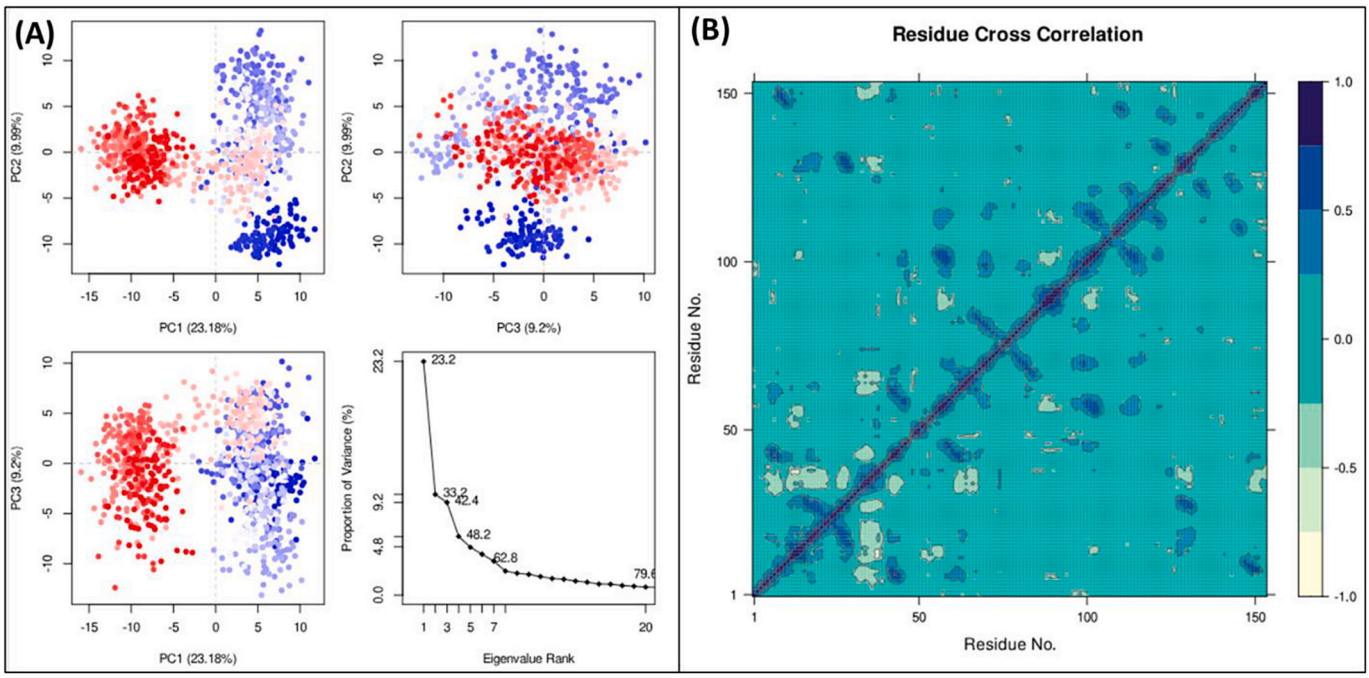

Fig. 18. (A) the eigenvalues of Principal Component Analysis (PCA) are plotted against the variance percentage of IL1β with Celastrol. The graph shows three distinct sections representing changing regions, with PC1, PC2, and PC3 contributing 23.18 %, 9.99 %, and 9.2 % to the total variance, respectively. (B) the IL1β-Celastrol dynamic cross-correlation map illustrates complex residue interactions, with cyan indicating positive correlations and purple indicating negative correlations.

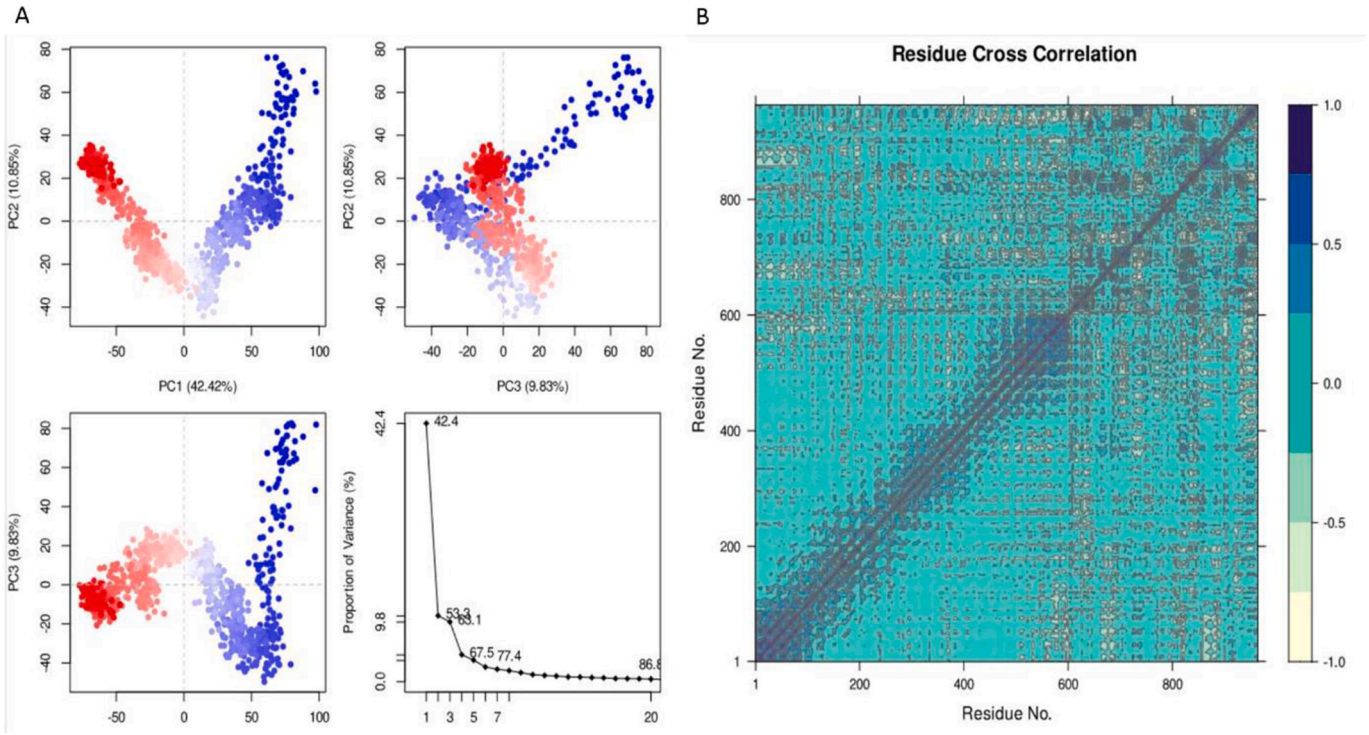

Fig. 19. (A) The eigenvalues of PCA are graphed against the variance percentage of the IL1β-Cefaclor Anhydrous complex, showing three distinct changing regions. Cumulatively, PC1, PC2, and PC3 contribute 17.53 %, 13.53 %, and 7.76 % to the total variance, respectively. (B) the dynamic cross-correlation map of the IL1β with Cefaclor Anhydrous complex illustrates complex residue interactions, with cyan representing positive correlations and purple indicating negative correlations.

the interaction networks. In this investigation, we analyzed miRNA and mRNA expression variations in blood samples, a non-invasive yet limited approach for TB biomarker detection. Future research may necessitate lung tissue samples for high-throughput sequencing profiling. Integrating these findings with dysregulated miRNA and gene analysis from lung tissue could validate potential biomarkers indicative of TB intracellular progression, promising prospects for future non-invasive diagnostics. While *Mtb* antigen-specific cellular responses show promise in detecting *Mtb* infection, they lack effectiveness in diagnosing tuberculosis [96]. This study establishes a basis for

Table 8
The average MM-GBSA binding energy calculation of Celastrol with IL1β was performed after every 10 ns from the MD Simulation trajectory.

Energies (Kcal/mol)	0ns	150ns
dG_{Bind}	−42.0907	−37.2472
dG_{Bind}_Lipo	−15.2074	−13.6799
dG_{Bind}_vdW	−34.357	−21.5752
dG_{Bind}_Coulomb	−20.0504	−20.5926
dG_{Bind}_H_{bond}	−1.74024	−2.4583
dG_{Bind}_Packing	−0.00033	−0.96811

Table 9
Average MM-GBSA binding energy calculation of Cefaclor Anhydrous with IL1β after every 10 ns from MD Simulation trajectorie

Energies (Kcal/mol)	0ns	150ns
dG_{Bind}	−27.8702	−35.6689
dG_{Bind}_Lipo	−12.7957	−4.68517
dG_{Bind}_vdW	−28.5405	−18.8577
dG_{Bind}_Coulomb	−32.3349	−31.8262
dG_{Bind}_H_{bond}	−2.15513	−2.57595
dG_{Bind}_Packing	−0.35303	−0.1223123

comparing different disease stages and identifies key biomarkers essential for accurately distinguishing between latent and active conditions. Future work will involve designing cohort studies using non-invasive blood samples to enhance these predictive models.

5. Conclusion

Several potential molecular markers, including PLEKHG1, CLPB, DOK4, IL1β, and TLR3, were predicted in this study, potentially aiding in the diagnosis and identification of therapeutic targets for LTB. We also identified Celastrol and Cefaclor Anhydrous drug as potential therapeutic agents for LTB treatment. Further research is needed to validate the sensitivity of these biomarkers in distinguishing various stages of TB and assessing the risk of progression from LTB to ATB.

CRediT authorship contribution statement

PhongSon Dinh: Writing – review & editing, Writing – original draft, Supervision, Software, Resources, Methodology, Funding acquisition, Formal analysis, Data curation. **ChauMyThanh Tran:** Visualization, Validation, Software, Resources, Formal analysis, Data curation. **ThiPhuongHoai Dinh:** Writing – review & editing, Supervision, Methodology, Investigation, Formal analysis, Data curation. **Hai-Anh Ha:** Visualization, Validation, Resources, Methodology. **Aigul Utegenova:** Writing – review & editing, Writing – original draft, Methodology, Formal analysis, Data curation, Conceptualization. **Awais Ali:** Writing – review & editing, Writing – original draft, Validation, Software, Resources, Investigation, Formal analysis, Data curation, Conceptualization. **Abdulaziz Alamri:** Resources, Project administration, Methodology, Funding acquisition, Formal analysis, Data curation.

Ethics statement

GEO belong to public datasets. The contributors to the database have obtained ethical approval. Thus, our research has no ethical issues.

Funding

This research has been funded by the Science Committee of the Ministry of Education and Science of the Republic of Kazakhstan (Grant No.AP13268846 ″New technologies for the pre-symptomatic diagnosis of tuberculosis and predicting the effectiveness of its treatment. Authors are thankful for Researchers Supporting Project number (RSPD2025R552), King Saud University, Riyadh, Saudi Arabia.

Declaration of competing interest

The authors declare that they have no known competing financial interests or personal relationships that could have appeared to influence the work reported in this paper.

Acknowledgments

The authors wish to thank Da Nang Lung Hospital for providing the data of their study. This research has been funded by the Science Committee of the Ministry of Education and Science of the Republic of Kazakhstan (Grant No.AP13268846 ″New technologies for the pre-symptomatic diagnosis of tuberculosis and predicting the effectiveness of its treatment”). Authors are thankful for Researchers Supporting Project number (RSPD2025R552), King Saud University, Riyadh, Saudi Arabia.

Appendix A. Supplementary data

Supplementary data to this article can be found online at https://doi.org/10.1016/j.bbrep.2025.101952.

Data availability

No data was used for the research described in the article.

References

[1] B.R. Bloom, A half-century of research on tuberculosis: successes and challenges, J. Exp. Med. 220 (2023), https://doi.org/10.1084/jem.20230859.
[2] World Health Organization, Global Tuberculosis Report 2021, 2021.
[3] W. Gong, X. Wu, Differential diagnosis of latent tuberculosis infection and active tuberculosis: a key to a successful tuberculosis control strategy, Front. Microbiol. 12 (2021) 745592, https://doi.org/10.3389/fmicb.2021.745592.
[4] K. Dheda, T. Perumal, H. Moultrie, R. Perumal, A. Esmail, A.J. Scott, The intersecting pandemics of tuberculosis and COVID-19: population-level and patient-level impact, clinical presentation, and corrective interventions, Lancet Respir. Med. 10 (6) (2022) 603–622, https://doi.org/10.1016/S2213-2600(22)00092-3.
[5] L. Zhuang, L. Yang, L. Li, Z. Ye, W. Gong, Mycobacterium tuberculosis: immune response, biomarkers, and therapeutic intervention, MedComm 5 (1) (2020) e419, https://doi.org/10.1002/mco2.419.
[6] I.A. Biraro, S. Kimuda, M. Egesa, S. Cose, E.L. Webb, M. Joloba, S.G. Smith, A. M. Elliott, H.M. Dockrell, A. Katamba, The use of Interferon gamma inducible protein 10 as a potential biomarker in the diagnosis of latent tuberculosis infection in Uganda, PLoS One 11 (2016) e0146098, https://doi.org/10.1371/journal.pone.0146098.
[7] K.L. Chin, L. Anibarro, M.E. Sarmiento, A. Acosta, Challenges and the way forward in diagnosis and treatment of tuberculosis infection, Trav. Med. Infect. Dis. 8 (2) (2023) 89, https://doi.org/10.3390/tropicalmed8020089.
[8] P. Stewart, S. Patel, A. Comer, S. Muneer, U. Nawaz, V. Quann, M. Bansal, V. Venketaraman, Role of B Cells in Mycobacterium tuberculosis infection, Vaccines (Basel) 11 (5) (2023) 955, https://doi.org/10.3390/vaccines11050955.
[9] Y.R. Patankar, R. Sutiwisesak, S. Boyce, R. Lai, C.S. Lindestam Arlehamn, A. Sette, S.M. Behar, Limited recognition of Mycobacterium tuberculosis-infected macrophages by polyclonal CD4 and CD8 T cells from the lungs of infected mice, Mucosal Immunol. 13 (1) (2020) 140–148, https://doi.org/10.1038/s41385-019-0217-6.
[10] H. Kim, S.J. Shin, Pathological and protective roles of dendritic cells in Mycobacterium tuberculosis infection: interaction between host immune responses and pathogen evasion, Front. Cell. Infect. Microbiol. 12 (2022) 891878, https://doi.org/10.3389/fcimb.2022.891878.
[11] M.L. Carabalí-Isajar, O.H. Rodríguez-Bejarano, T. Amado, M.A. Patarroyo, M. A. Izquierdo, J.R. Lutz, M. Ocampo, Clinical manifestations and immune response to tuberculosis, World J. Microbiol. Biotechnol. 39 (8) (2023) 206, https://doi.org/10.1007/s11274-023-03636-x.
[12] J.G. Burel, M. Pomaznoy, C.S. Lindestam Arlehamn, D. Weiskopf, R. da Silva Antunes, Y. Jung, M. Babor, V. Schulten, G. Seumois, J.A. Greenbaum, S. Premawansa, G. Premawansa, A. Wijewickrama, D. Vidanagama, B. Gunasena, R. Tippalagama, A.D. deSilva, R.H. Gilman, M. Saito, R. Taplitz, K. Ley, P. Vijayanand, A. Sette, B. Peters, Circulating T cell-monocyte complexes are markers of immune perturbations, Elife 8 (2019), https://doi.org/10.7554/eLife.46045.

[13] X. Wu, K. Liu, S. Li, Integrated bioinformatics analysis of dendritic cells hub genes reveal potential early tuberculosis diagnostic markers, BMC Med. Genom. 16 (1) (2023) 214, https://doi.org/10.1186/s12920-023-01646-0.

[14] S. Parlato, T. Chiacchio, D. Salerno, L. Petrone, L. Castiello, G. Romagnoli, I. Canini, D. Goletti, L. Gabriele, Impaired IFN-alpha-mediated signal in dendritic cells differentiates active from latent tuberculosis, PLoS One 13 (2018) e0189477, https://doi.org/10.1371/journal.pone.0189477.

[15] S. Mehra, D. Kaushal, Functional genomics reveals extended roles of the Mycobacterium tuberculosis stress response factor sigmaH, J. Bacteriol. 191 (2009) 3965–3980, https://doi.org/10.1128/JB.00064-09.

[16] Y. Rombouts, O. Neyrolles, The fat is in the lysosome: how Mycobacterium tuberculosis tricks macrophages into storing lipids, J. Clin. Investig. 133 (6) (2023) e168366, https://doi.org/10.1172/JCI168366.

[17] J. Buter, T.Y. Cheng, M. Ghanem, Mycobacterium tuberculosis releases an antacid that remodels phagosomes, Nat. Chem. Biol. 15 (2019), https://doi.org/10.1038/s41589-019-0336-0, 889-89.

[18] M.E. Pennini, R.K. Pai, D.C. Schultz, W.H. Boom, C.V. Harding, Mycobacterium tuberculosis 19-kDa lipoprotein inhibits IFN-gamma-induced chromatin remodeling of MHC2TA by TLR2 and MAPK signaling, J. Immunol. 176 (2006) 4323–4330, https://doi.org/10.4049/jimmunol.176.7.4323.

[19] M. Gough, D.K. Singh, B. Singh, D. Kaushal, S. Mehra, System-wide identification of myeloid markers of TB disease and HIV-induced reactivation in the macaque model of Mtb infection and Mtb/SIV co-infection, Front. Immunol. 13 (2022) 777733, https://doi.org/10.3389/fimmu.2022.777733.

[20] J.P. Zellweger, G. Sotgiu, M. Corradi, P. Durando, The diagnosis of latent tuberculosis infection (LTBI): currently available tests, future developments, and perspectives to eliminate tuberculosis (TB), Med. Lav. 111 (3) (2020) 170–183, https://doi.org/10.23749/mdl.v111i3.9983.

[21] World Health Organization, WHO Operational Handbook on Tuberculosis, Module 1: Prevention- Tuberculosis Preventive Treatment, 2020.

[22] R. Báez-Saldaña, L. García-García, L. Ferreyra-Reryes, P. Cruz-Hervert, N. Mongua-Rodríguez, G. Delgado-Sánchez, E. Ferreira-Guerrero, A. Rendón, Accuracy of the tuberculin skin test for diagnosis of latent tuberculosis in population with high coverage of Bacillus CalmetteÓ?Guérin vaccination, Rev. Méd. Hosp. Gen. México 83 (2020), https://doi.org/10.24875/hgmx.20000086.

[23] S. Nasreen, M. Shokoohi, M.S. Malvankar-Mehta, Prevalence of latent tuberculosis among health care workers in high burden countries: a systematic review and meta-analysis, PLoS One 11 (2016) e0164034, https://doi.org/10.1371/journal.pone.0164034.

[24] World Health Organization, WHO Consolidated Guidelines on Tuberculosis. Module 3: Diagnosis–Rapid Diagnostics for Tuberculosis Detection, 2020.

[25] A.E. Shapiro, J.M. Ross, M. Yao, I. Schiller, M. Kohli, N. Dendukuri, K.R. Steingart, D.J. Horne, Xpert MTB/RIF and Xpert Ultra assays for screening for pulmonary tuberculosis and rifampicin resistance in adults, irrespective of signs or symptoms, Cochrane Database Syst. Rev. 3 (2021) CD013694, https://doi.org/10.1002/14651858.CD013694.pub2.

[26] M.E. Ritchie, B. Phipson, D. Wu, Y. Hu, C.W. Law, W. Shi, G.K. Smyth, Limma powers differential expression analyses for RNA-sequencing and microarray studies, Nucleic Acids Res. 43 (2015) e47, https://doi.org/10.1093/nar/gkv007.

[27] M. Kohl, S. Wiese, B. Warscheid, Cytoscape: software for visualization and analysis of biological networks, Methods Mol. Biol. 696 (2011) 291–303, https://doi.org/10.1007/978-1-60761-987-1_18.

[28] M. Kutmon, F. Ehrhart, E.L. Willighagen, C.T. Evelo, S.L. Coort, CyTargetLinker app update: a flexible solution for network extension in Cytoscape, F1000Res 7 (2018), https://doi.org/10.12688/f1000research.14613.2.

[29] T. Danford, A. Rolfe, D. Gifford, GSE: a comprehensive database system for the representation, retrieval, and analysis of microarray data, Pac Symp. Biocomput. (2008) 539–550.

[30] J.C. Oliveros, Venny. An interactive tool for comparing lists with Venn's diagrams. https://bioinfogp.cnb.csic.es/tools/venny/index.html, 2007-2015.

[31] G. Yu, L.G. Wang, Y. Han, Q.Y. He, clusterProfiler: an R package for comparing biological themes among gene clusters, OMICS 16 (2012) 284–287, https://doi.org/10.1089/omi.2011.0118.

[32] S.L. Freshour, S. Kiwala, K.C. Cotto, A.C. Coffman, J.F. McMichael, J.J. Song, M. Griffith, O.L. Griffith, A.H. Wagner, Integration of the drug–gene interaction database (DGIdb 4.0) with open crowdsource efforts, Nucleic Acids Res. 49 (2021) D1144–D1151.

[33] O. Trott, A.J. Olson, AutoDock Vina: improving the speed and accuracy of docking with a new scoring function, efficient optimization, and multithreading, J. Comput. Chem. 31 (2010) 455–461.

[34] L.G. Ferreira, R.N. Dos Santos, G. Oliva, A.D. Andricopulo, Molecular docking and structure-based drug design strategies, Molecules 20 (2015) 13384–13421.

[35] M.P. Gajula, A. Kumar, J. Ijaq, Protocol for molecular dynamics simulations of proteins, Bio-protocol 6 (2016) e2051 e2051.

[36] B. Jawad, L. Poudel, R. Podgornik, N.F. Steinmetz, W.-Y. Ching, Molecular mechanism and binding free energy of doxorubicin intercalation in DNA, Phys. Chem. Chem. Phys. 21 (2019) 3877–3893.

[37] W. Tian, C. Chen, X. Lei, J. Zhao, J. Liang, CASTp 3.0: computed atlas of surface topography of proteins, Nucleic Acids Res. 46 (2018) W363–W367.

[38] S. Genheden, U. Ryde, The MM/PBSA and MM/GBSA methods to estimate ligand-binding affinities, Expet Opin. Drug Discov. 10 (2015) 449–461.

[39] I. Ali, M.A. Rasheed, S. Cavalu, K. Rahim, S. Ijaz, G. Yahya, L.P.W. Goh, M. S. Popoviciu, Identification of natural lead compounds against hemagglutinin-esterase surface glycoprotein in human coronaviruses investigated via MD simulation, principal component analysis, cross-correlation, H-bond plot and MMGBSA, Biomedicines 11 (2023) 793.

[40] B.J. Grant, A.P. Rodrigues, K.M. ElSawy, J.A. McCammon, L.S. Caves, Bio3d: an R package for the comparative analysis of protein structures, Bioinformatics 22 (2006) 2695–2696.

[41] S. Zhang, J.M. Krieger, Y. Zhang, C. Kaya, B. Kaynak, K. Mikulska-Ruminska, P. Doruker, H. Li, I. Bahar, ProDy 2.0: increased scale and scope after 10 years of protein dynamics modelling with Python, Bioinformatics 37 (2021) 3657–3659.

[42] M. de Martino, L. Lodi, L. Galli, E. Chiappini, Immune response to Mycobacterium tuberculosis: a narrative review, Front. Pediatr. 7 (2019) 350, https://doi.org/10.3389/fped.2019.00350.

[43] M. Herrera, Y. Keynan, P.J. McLaren, J.P. Isaza, B. Abrenica, L. López, D. Marin, Z. V. Rueda, Gene expression profiling identifies candidate biomarkers for new latent tuberculosis infections. A cohort study, PLoS One 17 (2022) e0274257.

[44] S.W. Lee, L.S. Wu, G.M. Huang, K.Y. Huang, T.Y. Lee, J.T. Weng, Gene expression profiling identifies candidate biomarkers for active and latent tuberculosis, BMC Bioinf. 17 (Suppl 1) (2016) 3, https://doi.org/10.1186/s12859-015-0848-x.

[45] N. Ponnusamy, M. Arumugam, Meta-analysis of active tuberculosis gene expression ascertains host directed drug targets, Front. Cell. Infect. Microbiol. 12 (2022) 1010771, https://doi.org/10.3389/fcimb.2022.1010771.

[46] O. Estevez, L. Anibarro, E. Garet, A. Pallares, L. Barcia, L. Calvino, C. Maueia, T. Mussa, F. Fdez-Riverola, D. Glez-Pena, M. Reboiro-Jato, H. Lopez-Fernandez, N. A. Fonseca, R. Reljic, A. Gonzalez-Fernandez, An RNA-seq based machine learning approach identifies latent tuberculosis patients with an active tuberculosis profile, Front. Immunol. 11 (2020) 1470, https://doi.org/10.3389/fimmu.2020.01470.

[47] J.D. Petrilli, L.E. Araujo, L.S. da Silva, A.C. Laus, I. Muller, R.M. Reis, E.M. Netto, L. W. Riley, S. Arruda, A. Queiroz, Whole blood mRNA expression-based targets to discriminate active tuberculosis from latent infection and other pulmonary diseases, Sci. Rep. 10 (2020) 22072, https://doi.org/10.1038/s41598-020-78793-2.

[48] M. Dutt, A. Kumar, M. Rout, B. Dehury, G. Martinez, P. Ndishimye, A.A. Kelvin, D. J. Kelvin, Drug repurposing for Mpox: discovery of small molecules as potential inhibitors against DNA-dependent RNA polymerase using molecular modeling approach, J. Cell. Biochem. 124 (2023) 701–715.

[49] T.A. Alandijany, M.M. El-Daly, A.M. Tolah, L.H. Bajrai, A.M. Khateb, G.S. Kumar, A. Dubey, V.D. Dwivedi, E.I. Azhar, A multi-targeted computational drug discovery approach for repurposing tetracyclines against monkeypox virus, Sci. Rep. 13 (2023) 14570.

[50] S. Yu, Y. Gao, J. Lu, Clinical profiles and related factors in tuberculosis patients with positive sputum smear mycobacterium tuberculosis tests, Sci. Rep. 14 (2024) 20376, https://doi.org/10.1038/s41598-024-71403-5.

[51] N. Orazulike, J. Sharma, S. Sharma, O.U. Umeora, Tuberculosis (TB) in pregnancy–a review, Eur. J. Obstet. Gynecol. Reprod. Biol. 259 (2021) 167–177.

[52] L. Pal, R. Nandani, P. Kumar, B. Swami, G. Roy, S. Bhaskar, Macrophages are the key players in promoting hyper-inflammatory response in a mouse model of TB-IRIS, Front. Immunol. 12 (2021) 775177.

[53] R. Gopalaswamy, S. Shanmugam, R. Mondal, S. Subbian, Of tuberculosis and non-tuberculous mycobacterial infections–a comparative analysis of epidemiology, diagnosis and treatment, J. Biomed. Sci. 27 (2020) 1–17.

[54] E.E. Hackett, H. Charles-Messance, S.M. O'Leary, L.E. Gleeson, N. Munoz-Wolf, S. Case, A. Wedderburn, D.G.W. Johnston, M.A. Williams, A. Smyth, M. Ouimet, K. J. Moore, E.C. Lavelle, S.C. Corr, S.V. Gordon, J. Keane, F.J. Sheedy, Mycobacterium tuberculosis limits host glycolysis and IL-1beta by restriction of PFK-M via MicroRNA-21, Cell Rep. 30 (2020) 124–136, https://doi.org/10.1016/j.celrep.2019.12.015, e4.

[55] P.T. Liu, M. Wheelwright, R. Teles, E. Komisopoulou, K. Edfeldt, B. Ferguson, M. D. Mehta, A. Vazirnia, T.H. Rea, E.N. Sarno, T.G. Graeber, R.L. Modlin, MicroRNA-21 targets the vitamin D-dependent antimicrobial pathway in leprosy, Nat. Med. 18 (2012) 267–273, https://doi.org/10.1038/nm.2584.

[56] N.C. Howard, N.D. Marin, M. Ahmed, B.A. Rosa, J. Martin, M. Bambouskova, A. Sergushichev, E. Loginicheva, N. Kurepina, J. Rangel-Moreno, L. Chen, B. N. Kreiswirth, R.S. Klein, J.M. Balada-Llasat, J.B. Torrelles, G.K. Amarasinghe, M. Mitreva, M.N. Artyomov, F.F. Hsu, B. Mathema, S.A. Khader, Mycobacterium tuberculosis carrying a rifampicin drug resistance mutation reprograms macrophage metabolism through cell wall lipid changes, Nat. Microbiol. 3 (2018) 1099–1108, https://doi.org/10.1038/s41564-018-0245-0.

[57] C. Keegan, S. Krutzik, M. Schenk, P.O. Scumpia, J. Lu, Y.L.J. Pang, B.S. Russell, K. S. Lim, S. Shell, E. Prestwich, D. Su, D. Elashoff, R.M. Hershberg, B.R. Bloom, J. T. Belisle, S. Fortune, P.C. Dedon, M. Pellegrini, R.L. Modlin, Mycobacterium tuberculosis transfer RNA induces IL-12p70 via synergistic activation of pattern recognition receptors within a cell network, J. Immunol. 200 (2018) 3244–3258, https://doi.org/10.4049/jimmunol.1701733.

[58] K.N. Schmidt, B. Leung, M. Kwong, K.A. Zarember, S. Satyal, T.A. Navas, F. Wang, P.J. Godowski, APC-independent activation of NK cells by the Toll-like receptor 3 agonist double-stranded RNA, J. Immunol. 172 (2004) 138–143, https://doi.org/10.4049/jimmunol.172.1.138.

[59] P. Stewart, S. Patel, A. Comer, S. Muneer, U. Nawaz, V. Quann, M. Bansal, V. Venketaraman, Role of B Cells in Mycobacterium tuberculosis infection, Vaccines (Basel) 11 (2023), https://doi.org/10.3390/vaccines11050955.

[60] M.R. Lee, L.Y. Chang, C.H. Chang, B.S. Yan, J.Y. Wang, W.H. Lin, Differed IL-1 beta response between active TB and LTBI cases by ex vivo stimulation of human monocyte-derived macrophage with TB-specific antigen, Dis. Markers 2019 (2019) 7869576.

[61] N.B.R. De Sá, N.C.S. de Souza, M. Neira-Goulart, M. Ribeiro-Alves, T.P. Da Silva, J. H. Pilotto, V.C. Rolla, C.B.W. Giacoia-Gripp, L.M. de Oliveira Pinto, D. Scott-Algara, M.G. Morgado, S.L.M. Teixeira, Inflammasome genetic variants are associated with tuberculosis, HIV-1 infection, and TB/HIV-immune reconstitution

inflammatory syndrome outcomes, Front. Cell. Infect. Microbiol. 12 (2022) 962059.
[62] N. Kaneko, M. Kurata, T. Yamamoto, The role of interleukin-1 in general pathology, Inflamm. Regen. 39 (2019) 12.
[63] K. Eislmayr, A. Bestehorn, L. Morelli, M. Borroni, L. Vande Walle, M. Lamkanfi, P. Kovarik, Nonredundancy of IL-1α and IL-1β is defined by distinct regulation of tissues orchestrating resistance versus tolerance to infection, Sci. Adv. 8 (2022) eabj7293.
[64] L. Huangfu, R. Li, Y. Huang, S. Wang, The IL-17 family in diseases: from bench to bedside, Signal Transduct. Targeted Ther. 8 (2023) 402.
[65] G. Mills, IL-17 and IL-17-producing cells in protection versus pathology, Nat. Rev. Immunol. 23 (2023) 38–54, https://doi.org/10.1038/s41577-022-00746-9.
[66] A. Halle, V. Hornung, G.C. Petzold, C.R. Stewart, B.G. Monks, T. Reinheckel, K. A. Fitzgerald, E. Latz, K.J. Moore, D.T. Golenbock, The NALP3 inflammasome is involved in the innate immune response to amyloid-beta, Nat. Immunol. 9 (2008) 857–865.
[67] M. Prabhavathi, B.S. Kabeer, A. Deenadayalan, A. Raja, Role of QuantiFERON-TB Gold antigen-specific IL-1β in diagnosis of active tuberculosis, Med. Microbiol. Immunol. 204 (2015) 567–574.
[68] X. Lu, S. Gong, X. Wang, N. Hu, D. Pu, J. Zhang, Y. Wang, J. Luo, Q. An, B. Ju, Celastrol exerts cardioprotective effect in rheumatoid arthritis by inhibiting TLR2/HMGB1 signaling pathway-mediated autophagy, Int. Arch. Allergy Immunol. 182 (2021) 1245–1254.
[69] J. Yang, J. Liu, J. Li, M. Jing, L. Zhang, M. Sun, Q. Wang, H. Sun, G. Hou, C. Wang, Celastrol inhibits rheumatoid arthritis by inducing autophagy via inhibition of the PI3K/AKT/mTOR signaling pathway, Int. Immunopharmacol. 112 (2022) 109241.
[70] G. Li, D. Liu, Y. Zhang, Y. Qian, H. Zhang, S. Guo, M. Sunagawa, T. Hisamitsu, Y. Liu, Celastrol inhibits lipopolysaccharide-stimulated rheumatoid fibroblast-like synoviocyte invasion through suppression of TLR4/NF-κB-mediated matrix metalloproteinase-9 expression, PLoS One 8 (2013) e68905.
[71] V.K.W. Wong, C. Qiu, S.W. Xu, B.Y.K. Law, W. Zeng, H. Wang, F. Michelangeli, I.R. D.S.R. Dias, Y.Q. Qu, T.W. Chan, Ca2+ signalling plays a role in celastrol-mediated suppression of synovial fibroblasts of rheumatoid arthritis patients and experimental arthritis in rats, Br. J. Pharmacol. 176 (2019) 2922–2944.
[72] Y. Wang, Q. Liu, H. Chen, J. You, B. Peng, F. Cao, X. Zhang, Q. Chen, G. Uzan, L. Xu, Celastrol improves the therapeutic efficacy of EGFR-TKIs for non-small-cell lung cancer by overcoming EGFR T790M drug resistance, Anti Cancer Drugs 29 (2018) 748–755.
[73] T. Bufu, X. Di, Z. Yilin, L. Gege, C. Xi, W. Ling, Celastrol inhibits colorectal cancer cell proliferation and migration through suppression of MMP3 and MMP7 by the PI3K/AKT signaling pathway, Anti Cancer Drugs 29 (2018) 530–538.
[74] S. Bo, C. Haibin, Z. Hongguang, W. Mianhua, Celastrol induces caspase-dependent apoptosis of hepatocellular carcinoma cells by suppression of mammalian target of rapamycin, J. Tradit. Chin. Med. 41 (2021).
[75] D. Zhan, T. Ni, H. Wang, M. Lv, M. Sunagawa, Y. Liu, Celastrol inhibits the proliferation and decreases drug resistance of cisplatin-resistant gastric cancer SGC7901/DDP cells, Anti Cancer Agents Med. Chem. 22 (2022) 270–279.
[76] M.K. Shanmugam, K.S. Ahn, J.H. Lee, R. Kannaiyan, N. Mustafa, K.A. Manu, K. S. Siveen, G. Sethi, W.J. Chng, A.P. Kumar, Celastrol attenuates the invasion and migration and augments the anticancer effects of bortezomib in a xenograft mouse model of multiple myeloma, Front. Pharmacol. 9 (2018) 365.
[77] C-j Zhang, N. Zhu, J. Long, H-t Wu, Y-x Wang, B-y Liu, D-f Liao, L. Qin, Celastrol induces lipophagy via the LXRα/ABCA1 pathway in clear cell renal cell carcinoma, Acta Pharmacol. Sin. 42 (2021) 1472–1485.
[78] N. Ji, J. Li, Z. Wei, F. Kong, H. Jin, X. Chen, Y. Li, Y. Deng, Effect of celastrol on growth inhibition of prostate cancer cells through the regulation of hERG channel in vitro, BioMed Res. Int. 2015 (2015).
[79] H. Li, J. Zhang, L. Sun, B. Li, H. Gao, T. Xie, N. Zhang, Z. Ye, Celastrol induces apoptosis and autophagy via the ROS/JNK signaling pathway in human osteosarcoma cells: an in vitro and in vivo study, Cell Death Dis. 6 (2015) e1604 e1604.
[80] S. Shrivastava, M.K. Jeengar, V.S. Reddy, G.B. Reddy, V. Naidu, Anticancer effect of celastrol on human triple negative breast cancer: possible involvement of oxidative stress, mitochondrial dysfunction, apoptosis and PI3K/Akt pathways, Exp. Mol. Pathol. 98 (2015) 313–327.
[81] H. Zhang, J. Li, G. Li, S. Wang, Effects of celastrol on enhancing apoptosis of ovarian cancer cells via the downregulation of microRNA-21 and the suppression of the PI3K/Akt-NF-κB signaling pathway in an in vitro model of ovarian carcinoma, Mol. Med. Rep. 14 (2016) 5363–5368.
[82] Z. Cha, J. Cheng, H. Xiang, J. Qin, Y. He, Z. Peng, J. Jia, H. Yu, Celastrol enhances TRAIL-induced apoptosis in human glioblastoma via the death receptor pathway, Cancer Chemother. Pharmacol. 84 (2019) 719–728.
[83] X. Li, H. Wang, J. Ding, S. Nie, L. Wang, L. Zhang, S. Ren, Celastrol strongly inhibits proliferation, migration and cancer stem cell properties through suppression of Pin1 in ovarian cancer cells, Eur. J. Pharmacol. 842 (2019) 146–156.
[84] Y.S. Alqahtani, B.A. Alyami, A.O. Alqarni, M.H. Mahnashi, A. Ali, Q. Javed, M. Hassan, M. Ehsan, Cephalosporin as potent urease and tyrosinase inhibitor: exploration through enzyme inhibition, kinetic mechanism, and molecular docking studies, BioMed Res. Int. 2022 (2022).
[85] A.-S. Mohammad, Antimicrobial susceptibility of Escherichia coli isolates from clinical specimens in children over a 5-year period in Jordan, Biomed. Pharmacol. J. 9 (2016) 9–13.
[86] J. Prajapati, P. Rao, L. Poojara, D. Acharya, S.K. Patel, D. Goswami, R.M. Rawal, A comprehensive in vitro and in silico assessment on inhibition of CYP51B and ergosterol biosynthesis by eugenol in rhizopus oryzae, Curr. Microbiol. 80 (2023) 47.
[87] P. Rao, D. Goswami, R.M. Rawal, Molecular insights on ar-turmerone as a structural, functional and pharmacophoric analogue of synthetic mosquito repellent DEET by comprehensive computational assessment, Sci. Rep. 12 (2022) 15564.
[88] P. Rao, D. Goswami, R.M. Rawal, Extending the lore of curcumin as dipteran Butyrylcholine esterase (BChE) inhibitor: a holistic molecular interplay assessment, PLoS One 17 (2022) e0269036.
[89] L.L. Ferreira, A.D. Andricopulo, ADMET modeling approaches in drug discovery, Drug Discov. Today 24 (2019) 1157–1165.
[90] I. Saleem Naz Babari, M. Islam, H. Saeed, H. Nadeem, F. Imtiaz, A. Ali, I. Ahmad, Design, synthesis, in-vitro biological profiling and molecular docking of some novel oxazolones and imidazolones exhibiting good inhibitory potential against acetylcholine esterase, J. Biomol. Struct. Dyn. (2024) 1–18.
[91] E. Nwanna, R. Ojo, N. Shafiq, A. Ali, E. Okello, G. Oboh, An in silico in vitro and in vivo study on the influence of an eggplant fruit (Solanum Anguivi Lam) diet on metabolic dysfunction in the sucrose-induced diabetic-like fruit fly (Drosophila Melanogaster), Foods 13 (4) (2024) 559.
[92] N. Shafiq, M. Arshad, A. Ali, F. Rida, M. Mohany, U. Arshad, M. Milošević, Integrated computational modeling and in-silico validation of flavonoids-Alliuocide G and Alliuocide A as therapeutic agents for their multi-target potential: combination of molecular docking, MM-GBSA, ADMET and DFT analysis, South Afr. J. Bot. 169 (2024) 276–300.
[93] P. Dinh, C. Tran, T. Dinh, A. Ali, S. Pan, Hsa_circRNA_0000284 acts as a ceRNA to participate in coronary heart disease progression by sponging miRNA-338-3p via regulating the expression of ETS1, J. Biomol. Struct. Dyn. 42 (10) (2024) 5114–5127.
[94] R. Riaz, S. Parveen, N. Shafiq, A. Ali, M. Rashid, Virtual screening, ADME prediction, drug-likeness, and molecular docking analysis of Fagonia indica chemical constituents against antidiabetic targets, Mol. Divers. (2024) 1–22.
[95] A. Ali, A. Alamri, A. Hajar, NK/DC crosstalk-modulating antitumor activity via Sema3E/PlexinD1 axis for enhanced cancer immunotherapy, Immunol. Res. (2024) 1–12, https://doi.org/10.1007/s12026-024-09536-y.
[96] Q. Yang, Q. Chen, M. Zhang, Y. Cai, F. Yang, J. Zhang, G. Deng, T. Ye, Q. Deng, G. Li, H. Zhang, Y. Yi, R.P. Huang, X. Chen, Identification of eight-protein biosignature for diagnosis of tuberculosis, Thorax 75 (2020) 576–583, https://doi.org/10.1136/thoraxjnl-2018-213021.